Western Michigan University
ScholarWorks at WMU

Dissertations | Graduate College

12-1997

Collision Spectroscopy of Low Energy Capture by Multiply Charged Ions from Atomic Targets

Kadir Akgungor
Western Michigan University

Follow this and additional works at: https://scholarworks.wmich.edu/dissertations

 Part of the Physics Commons

Recommended Citation

Akgungor, Kadir, "Collision Spectroscopy of Low Energy Capture by Multiply Charged Ions from Atomic Targets" (1997). *Dissertations*. 1653.
https://scholarworks.wmich.edu/dissertations/1653

This Dissertation-Open Access is brought to you for free and open access by the Graduate College at ScholarWorks at WMU. It has been accepted for inclusion in Dissertations by an authorized administrator of ScholarWorks at WMU. For more information, please contact wmu-scholarworks@wmich.edu.

COLLISION SPECTROSCOPY OF LOW ENERGY CAPTURE BY MULTIPLY CHARGED IONS FROM ATOMIC TARGETS

by

Kadir Akgungor

A Dissertation
Submitted to the
Faculty of The Graduate College
in partial fulfillment of the
requirements for the
Degree of Doctor of Philosophy
Department of Physics

Western Michigan University
Kalamazoo, Michigan
December 1997

Reproduced with permission of the copyright owner. Further reproduction prohibited without permission.

COLLISION-SPECTROSCOPY OF LOW ENERGY CAPTURE BY MULTIPLY CHARGED IONS FROM ATOMIC TARGETS

Kadir Akgungor, Ph.D.

Western Michigan University, 1997

State-selective differential cross sections for single-electron capture processes in very slow collisions of Ar^{q+} (q = 4 - 6) ions with Ne, and Ar^{6+} ions with He have been studied experimentally at laboratory collision energies between 15 and 100 qeV, and at scattering angles between 0° and 8° by means of translational energy-gain spectroscopy technique. The translational energy spectra show that only a few final states are populated depending on the charge state of the projectile, the projectile laboratory scattering angle, and the collision energy. These measurements also show that the dominant reaction channels are due to capture into excited states of the projectile product $Ar^{(q-1)+}$. However, at very low energies, other channels due to transfer excitation processes are found to open at large scattering angles. The energy-gain spectra are interpreted qualitatively in terms of the reaction windows, which are calculated using the single-crossing Landau-Zener model and the extended version of the classical over barrier model. The energy dependence of cross sections for single-electron capture by Ar^{q+} (q = 4 - 8) ions from He and Ne are also measured and found to be nearly independent of collision energy, but increase with the projectile charge state. The data are also compared with other available measurements and theoretical calculations.

Reproduced with permission of the copyright owner. Further reproduction prohibited without permission.

INFORMATION TO USERS

This manuscript has been reproduced from the microfilm master. UMI films the text directly from the original or copy submitted. Thus, some thesis and dissertation copies are in typewriter face, while others may be from any type of computer printer.

The quality of this reproduction is dependent upon the quality of the copy submitted. Broken or indistinct print, colored or poor quality illustrations and photographs, print bleedthrough, substandard margins, and improper alignment can adversely affect reproduction.

In the unlikely event that the author did not send UMI a complete manuscript and there are missing pages, these will be noted. Also, if unauthorized copyright material had to be removed, a note will indicate the deletion.

Oversize materials (e.g., maps, drawings, charts) are reproduced by sectioning the original, beginning at the upper left-hand corner and continuing from left to right in equal sections with small overlaps. Each original is also photographed in one exposure and is included in reduced form at the back of the book.

Photographs included in the original manuscript have been reproduced xerographically in this copy. Higher quality 6" x 9" black and white photographic prints are available for any photographs or illustrations appearing in this copy for an additional charge. Contact UMI directly to order.

UMI

A Bell & Howell Information Company
300 North Zeeb Road, Ann Arbor MI 48106-1346 USA
313/761-4700 800/521-0600

Reproduced with permission of the copyright owner. Further reproduction prohibited without permission.

Reproduced with permission of the copyright owner. Further reproduction prohibited without permission.

UMI Number: 9813576

UMI Microform 9813576
Copyright 1998, by UMI Company. All rights reserved.

This microform edition is protected against unauthorized
copying under Title 17, United States Code.

UMI
300 North Zeeb Road
Ann Arbor, MI 48103

Reproduced with permission of the copyright owner. Further reproduction prohibited without permission.

Copyright by
Kadir Akgungor
1997

Reproduced with permission of the copyright owner. Further reproduction prohibited without permission.

ACKNOWLEDGMENTS

I would like to express my gratitude to my adviser Dr. E. Y. Kamber for his guidance, encouragement and support during the course of this study.

I would like to thank the committee members, Dr. N. Berrah, Dr. T. Gorczyca, Dr. D. Halderson, Dr. P. Merati, and Dr. J. A. Tanis for their comments and review of this dissertation.

I wish to thank Dr. S. Ferguson for his valuable help and guidance at the WMU accelerator laboratory and for his friendship. Also, I would like to acknowledge Mr. J. Cornell and Mr. R. Hiltbrand for their help and lessons in the work shop. For carefully reading this dissertation and their valuable suggestions, I would like to express my appreciation to Dr. G. Toth and Dr. T. Gorczyca.

Finally, I would like to thank my entire family, my wife Sedef, my daughter Evrim, my father M. Nevzat (unfortunately, he could not see my graduation), my mother Seher, my sisters, nephews and niece, and my parents in law, Sezer and Uner Birkan for being patient and for their endless support that enabled me to complete this degree.

Kadir Akgungor

Reproduced with permission of the copyright owner. Further reproduction prohibited without permission.

TABLE OF CONTENTS

Reproduced with permission of the copyright owner. Further reproduction prohibited without permission.

Table of Contents - Continued

CHAPTER

Reproduced with permission of the copyright owner. Further reproduction prohibited without permission.

LIST OF TABLES

Reproduced with permission of the copyright owner. Further reproduction prohibited without permission.

LIST OF FIGURES

Reproduced with permission of the copyright owner. Further reproduction prohibited without permission.

List of Figures - Continued

Reproduced with permission of the copyright owner. Further reproduction prohibited without permission.

Reproduced with permission of the copyright owner. Further reproduction prohibited without permission.

Reproduced with permission of the copyright owner. Further reproduction prohibited without permission.

CHAPTER I

INTRODUCTION

Among the principal topics for research in atomic physics is the study of collisions involving atomic and molecular particles. Three fundamental atomic processes may occur as a result of ion-atom collisions: excitation, ionization, and electron capture. Fast electronic timing techniques allow one to design experiments so that individual atomic processes can be isolated and examined. Of particular interest is single-electron capture from neutral target atoms by multiply-charged ions since this is the predominant reaction for low-energy collisions. When low-energy multiply-charged ions collide with atomic targets, electron capture may take place through a variety of reaction channels. These include single- and multiple-electron capture, electron capture accompanied by target excitation or ionization, and simultaneous electron capture and projectile excitation.

The reasons for the study of electron capture processes involving multiply-charged ion-atom collisions range from interest in pure science to making a new laser. Electron capture processes involving multiply charged ions are of interest in the study of astrophysical plasmas, where they have been found to modify the ionization structure of plasmas and exert a major influence on plasmas created by the absorption of high frequency radiation (Pequignot, 1980). Another important application is the development of techniques for controlled thermonuclear fusion (Meade, 1974). In addition, neon is

Reproduced with permission of the copyright owner. Further reproduction prohibited without permission.

frequently introduced in Tokamak devices as a diagnostic element for fusion plasmas. Also, it is important to have the data for the collision of low-energy multiply-charged ions with neutral atoms to test the existing theoretical models of atomic structure and low-energy collision mechanisms and to build more realistic models.

In recent years, considerable attention has been directed to single-electron capture by low-energy multiply-charged ions from neutral targets (Giese et al., 1986; Kamber, 1988; Andersson et al., 1991; Justiniano et al., 1984; Okuno et al., 1995; Yaltkaya et al., 1993). However, in spite of the experimental and theoretical work which has been done in this field, there is much to be learned concerning the details of electron capture and related processes in low-energy ion-atom collisions. Although a large number of total cross sections have been measured for single-electron capture by multiply charged ions (Justiniano et al., 1984; Okuno et al., 1995; Suziki et al., 1997), relatively little work has been done on the doubly differential cross section measurements in the low-energy region (Yaltkaya et al., 1993; Biederman et al., 1990). Such studies can contribute significantly to the understanding of ion-atom collisions. For example, doubly differential studies provide more information about the nature of the interaction than the measurements of total cross sections alone, and can provide a test of the applicability of various theoretical models.

Previous measurements of single-electron capture by multiply-charged argon ions from neon have been reported by several investigators. Cocke et al. (1981) have used a secondary ion recoil source to study electron capture and ionization in collisions of Ar^{q+} ($q = 1 - 9$) with He, Ne, Ar, and Xe at projectile energies between 250 and 660 eV per

Reproduced with permission of the copyright owner. Further reproduction prohibited without permission.

charge. By analyzing outgoing projectiles and target ions in coincidence they have measured cross sections for direct ionization, electron capture, and transfer ionization. Nielsen et al. (1984) measured absolute state-selective single-electron capture cross sections for 200, 500, and 1000 eV Ar^{6+} ions on Ne and Ar by means of energy-gain spectroscopy. Liljeby et al. (1986) have measured absolute cross sections for single- and multi-electron processes in 1.8 qkeV Ar^{q+} (q = 1 -9) - Ne, Ar and Kr collisions. Kamber (1988) has measured single- and double-electron capture into selected states by means of translational energy spectroscopy for collisions of 12 keV Ar^{4+} and 15 keV Ar^{5+} ions with He, Ne, Ar and Kr. Lee et al. (1995) have obtained translational energy spectra for single-electron capture by 8 keV Ar^{4+} ions in He, Ne and Ar using a double-focusing translational energy spectrometer. Very recently, Suzuki et al. (1997) have measured total cross sections for single- and multiple-charge changing of Ar^{q+} (q = 4 - 9) in collisions with Ne at very low impact energies ranging from 0.0125 to 25 qeV/amu.

In this work we have studied doubly differential cross sections, in energy and angle, for state-selective single-electron capture processes in collisions of low-energy multiply-charged argon ions with He and Ne targets by applying the collision spectroscopy technique. Collision spectroscopy consists of measuring doubly differential cross sections, in translational energy-gain (or loss) and projectile scattering angles, using the energy gain/loss technique. Such a technique is utilized to measure the total change in internal energy of the colliding system that takes place during the collision. The measured translational energy gain or loss spectrum usually reveals information on the states of the participating particles, as well as their partial cross sections. Also, measuring

Reproduced with permission of the copyright owner. Further reproduction prohibited without permission.

the projectile scattering angle gives information on the dynamics of the populated states. Additionally, the energy gained by the projectile is kinematically related to both the change of electronic energy during the reaction and the projectile scattering angle. Thus, measurement of both parameters is informative.

The goals of this study are to measure the translational energy-gain spectra, the differential cross sections, and the total cross sections for single-electron capture in collisions of Ar^{q+} ions (q = 4 - 8) with He and Ne at collision energies between 15 and 100 qeV and at scattering angles between 0° and 8°. The measurements will be compared to several theoretical models. Energy-gain spectra will be compared to the predictions of a single-crossing Landau-Zener model (Landau, 1932; Zener, 1932) and to the predictions of an extended version of the classical over barrier (ECOB) model (Niehaus, 1986). Differential cross sections will be compared to the multistate collision model (Salop et al., 1976), while total cross sections will be compared to the predictions of multichannel Landau Zener (MCLZ) model, absorbing sphere model (Olson et al., 1976), Muller-Salzborn scaling law (Muller et al., 1977) and classical over barrier model (COB) (Ryufuku et al., 1980; Mann et al., 1981).

The contents of this dissertation are as follows. After an introduction in the first chapter, the second chapter will be devoted to an explanation of the theoretical models used in this dissertation. The experimental apparatus and data analysis are presented, respectively, in Chapters III and IV . In Chapter V, the experiment results, discussion of the results and comparison to theoretical models will be presented. A conclusion is given in Chapter VI.

Reproduced with permission of the copyright owner. Further reproduction prohibited without permission.

CHAPTER II

THEORETICAL CONSIDERATIONS

Single-electron capture is the most probable process in low-energy multiply charged ion-atom collisions (Kamber et al., 1991). This collision may be represented by the equation

$$A^{q+}(n_o,l_o,m_o) + B \rightarrow A^{(q-1)+}(n,l,m) + B^{+} + \Delta E \qquad (2.1)$$

where q is the initial charge state of the projectile ion A, ΔE is the energy defect of the reaction, and (n_o,l_o,m_o) and (n,l,m) are, respectively, the quantum numbers of the initial and final states of the projectile ion.

Besides single-electron capture, transfer ionization is also significant in some collision systems. Transfer ionization is the process whereby double-electron capture occurs to doubly excited states followed by the loss of one projectile electron via autoionization. Since after a transfer ionization event the projectile ion has a charge state changed by one unit, transfer ionization can appear as a single-electron capture under charge state analysis.

The focus of this chapter is the theoretical models used to study single-electron capture by multiply charged ions from target atoms at low collision energies. The emphasis will be on those models which are related to the prediction of the final state

Reproduced with permission of the copyright owner. Further reproduction prohibited without permission.

populations of the captured electrons, differential cross sections, and total cross sections for single-electron capture.

Kinematics

In a classical two-body collision, the translational energy E of an ion following an inelastic scattering process differs from the energy E_o of the projectile ion by

$$E - E_o = \Delta E - \Delta K = Q \qquad (2.2)$$

where ΔK is the translational energy given to the target, ΔE is the energy defect of the reaction, and Q is the total change in internal energy that takes places during the inelastic collision. The parameter Q is the energy gained by of the projectile ion during a collision, usually called the Q-value of the reaction, and can be negative or positive depending on the binding energy of the captured electron. The parameter ΔE is calculated according to the formula

$$\Delta E = I_p(A^{(q-1)+}) - I_p(B) - E_x \qquad (2.3)$$

where $I_p(A^{(q-1)+})$ and $I_p(B)$ are, respectively, the ionization potentials of the projectile product ion $A^{(q-1)+}$ and the target atom B, and E_x is the excitation energy of the xth level of projectile product ion $A^{(q-1)+}$ or target product ion B^+.

The translational energy ΔK given to the target is calculated according to the formula,

Reproduced with permission of the copyright owner. Further reproduction prohibited without permission.

$$\Delta K = \frac{m_p}{m_p+M}(1 - \cos\theta_p)\left[\frac{2ME_o}{m_p+M} - \Delta E\right] + \frac{m_p(\Delta E)^2}{4ME_o}\cos\theta_p \qquad (2.4)$$

where θ_p is the laboratory scattering angle of the projectile, and m_p and M are, respectively, the projectile and target masses (Cooks, 1978). A typical charge exchange reaction at low collision energy in the laboratory frame of reference is shown in Figure 1, in which the projectile ion is scattered through an angle θ_p while the recoil target ion is scattered through an angle θ_r.

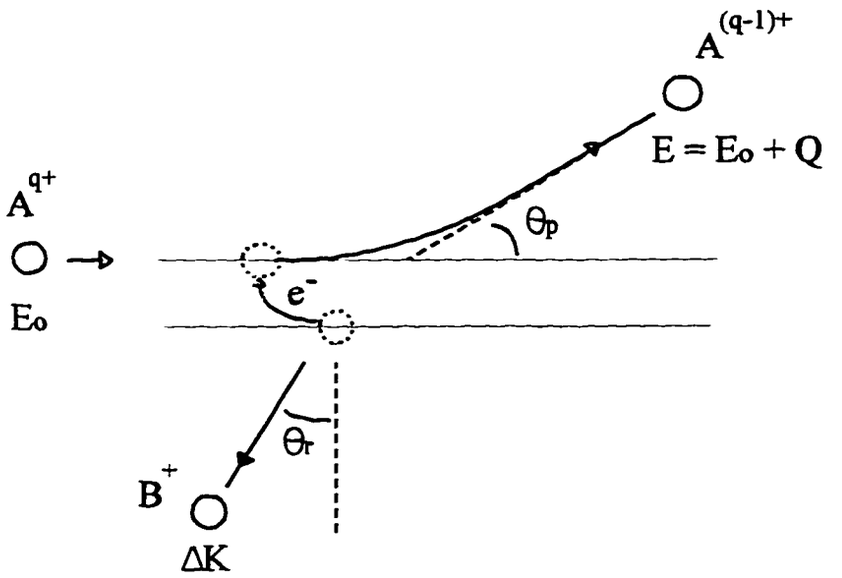

Figure 1. Typical Electron Capture Reaction in the Laboratory Frame.

If the scattering angle θ_p of the projectile is close to zero, ΔK can be approximated by

Reproduced with permission of the copyright owner. Further reproduction prohibited without permission.

$$\Delta K = \frac{m_p(\Delta E)^2}{4ME_o} . \qquad (2.5)$$

This quantity ΔK, at low energies and for heavy projectile ions in collision with light targets, has been observed by Kamber et al. (1987) in O^{2+} - He collisions as a relative shift of about 0.7 eV in the energy-gain of the ^2P capture channel going from scattering angle 0° to 2°.

Landau-Zener Model

In the process of single-electron capture by a multiply-charged ion in collision with a neutral atom, the two collision by products have positive charges; therefore the interaction between them is repulsive. Before the electron capture, however, the ion-atom interaction is a relatively weak polarization attraction at large internuclear separations. Thus electron capture in ion-atom collisions has been recognized as a typical example of a reaction which can proceed through curve-crossing. According to the curve-crossing picture of the electron capture process the transition from initial to final state occurs near the curve crossing point of a pair of molecular potential energy curves which correspond to different separated-atom states, i.e. ingoing and outgoing channels.

During a collision, slow reactants are described as forming a quasimolecule whereby atomic energy levels are connected by way of molecular ones. Charge transfer occurs between these molecular electronic states. Potential curves describing the behavior of the ion-atom system during the collision may be determined by solving the Schrodinger

Reproduced with permission of the copyright owner. Further reproduction prohibited without permission.

equation for the molecular electronic states. The potential curves obtained are adiabatic in the sense that they are prohibited from crossing one another. This is the consequence of the Neumann-Wigner non-crossing rule that does not allow molecular energy levels of the same symmetry to cross. However, certain other types of potential curves are allowed to pass through each other due to the strong interaction between the two. These diabatic curves violate the non-crossing rule, but they are often used to describe charge transfer reactions. In Figure 2 representative adiabatic (dashed lines) and diabatic (solid lines) curves are shown.

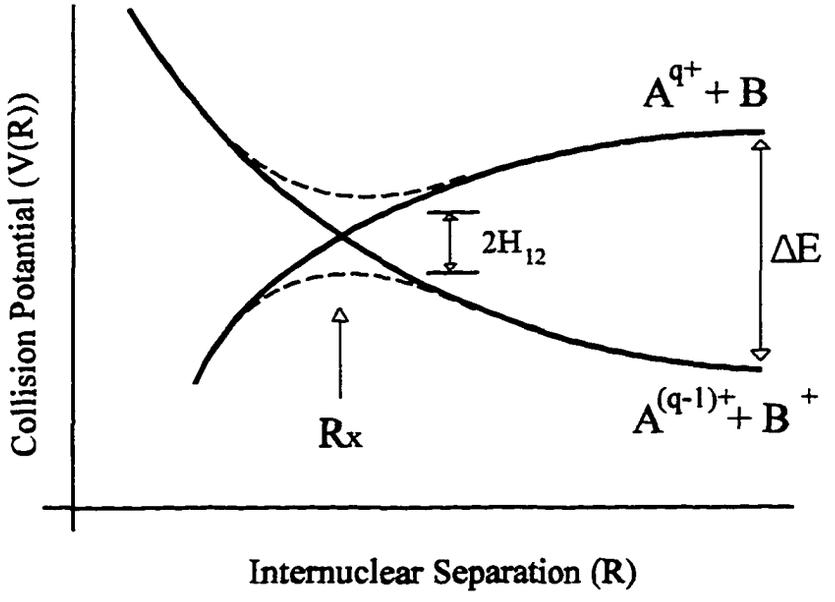

Figure 2. A Representative Plot of the Potential Curves Versus Internuclear Separation. Solid Lines are Diabatic and Dashed Lines are Adiabatic Potential Curves Near the Curve Crossing Point R_x.

The earliest theoretical work on curve-crossing was done by Landau (1932) and Zener (1932), who independently derived the well-known formula for the transition

Reproduced with permission of the copyright owner. Further reproduction prohibited without permission.

probability which bears their names. In this model, the transition from initial to final state is assumed to occur at the crossing point of a pair of diabatic potential energy curves which correspond to ingoing ($A^{q+} + B$) and outgoing ($A^{(q-1)+} + B^-$) channels.

In the Landau-Zener model, the single-crossing probability at each crossing point R_x is given by the following formula (Zener, 1932; Landau, 1932)

$$P_n = \exp\left[\frac{-2\pi H_{12}^2}{v_r \Delta F}\right] \tag{2.6}$$

where H_{12} is the coupling matrix element and is approximately equal to one-half the adiabatic splitting at the curve crossing R_x (see Figure 2); and ΔF is the difference in slopes of the diabatic potential curves (solid curves) at the curve-crossing. If one assumes a repulsive Coulomb interaction U_1 in the outgoing channel and zero interaction U_2 in the incoming channel, it is possible to represent ΔF by

$$\Delta F = \frac{d}{dR}[U_1(R) - U_2(R)]\Big|_{R=R_x} \propto \frac{q-1}{R^2} \tag{2.7}$$

where q is the charge state of the incident ion. In the straight-line trajectory approximation the radial velocity v_r at the curve crossing R_x is given by

$$v_r = v_o\left[1 - \left(\frac{b}{R_x}\right)^2\right]^{\frac{1}{2}} \tag{2.8}$$

where b is the impact parameter and v_o is the relative velocity (Kimura et al, 1984). As

Reproduced with permission of the copyright owner. Further reproduction prohibited without permission.

always, the most difficult problem is in developing a formulation for the coupling matrix elements that can be easily applied from case to case. Olson and Salop (1976) have developed a semiempirical expression for the coupling matrix element applicable to collisions of fully-ionized ions with hydrogen atoms. Their expression is

$$H_{12}^{os} = 9.13\, q^{-\frac{1}{2}} \exp\left[-1.324\, \alpha R_x q^{-\frac{1}{2}}\right] \tag{2.9}$$

where

$$\alpha = (2I_t)^{-\frac{1}{2}} \tag{2.10}$$

and I_t is the ionization potential of the target in atomic units. Kimura et al. (1984) have reduced the coefficient of this coupling matrix element by 40%, i.e., to 5.48, in order to get good agreement with their measurements.

The probability of electron transfer for each projectile curve is P = p(1-p) where p is the probability that when traversing the crossing the system remains on the same potential curve, and (1-p) is the probability for a jump from one curve to the other curve. Since there are two possible ways of traversing the potential (capture on the way in or on the way out, see Figure 3), the total probability at a given impact parameter for two states and a single crossing is given by

$$P = 2p(1 - p) \tag{2.11}$$

The extension of the Landau-Zener model to multichannel system (see Figure 4) has been carried out by Salop and Olson (1976). Assuming that there is no interference between

Reproduced with permission of the copyright owner. Further reproduction prohibited without permission.

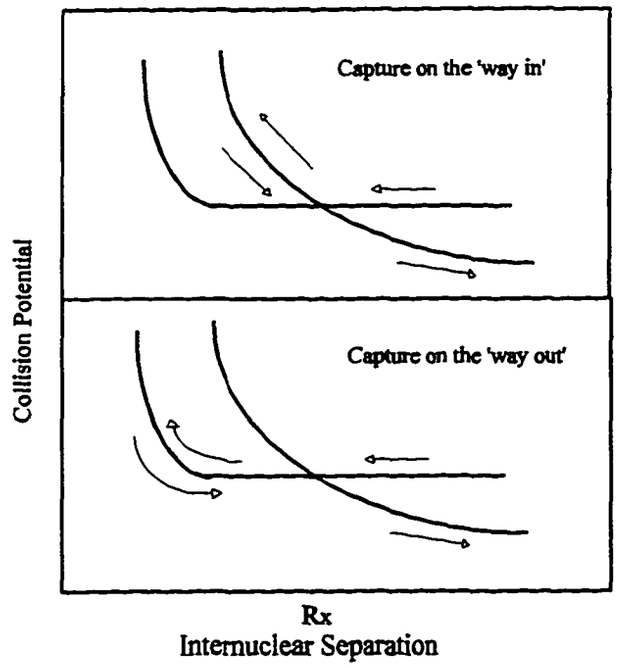

Figure 3. Two-State Picture of Trajectories for Capture on the Way-in and Capture on the Way-out.

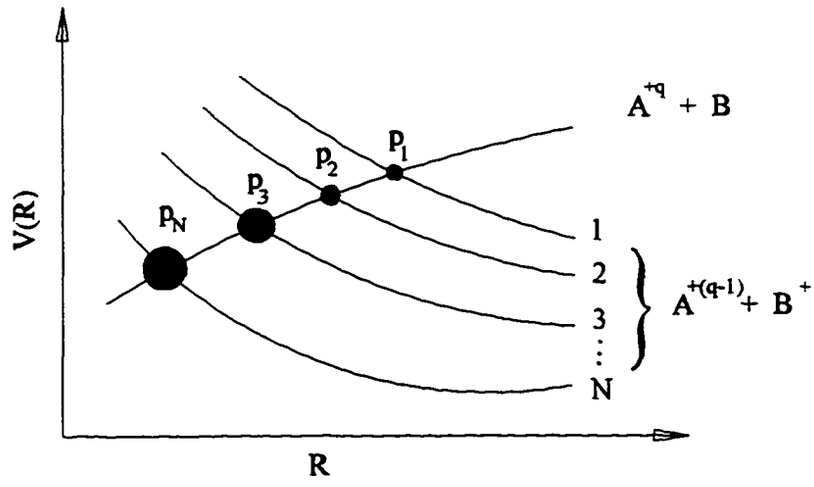

Figure 4. Schematic Representation for the Potential Curves of Single-Electron Capture in A^{q+} + B Collision.

Reproduced with permission of the copyright owner. Further reproduction prohibited without permission.

different paths leading to a particular final state, the probability P_n (n = 1,2,....N) for capture into the nth final state is

$$\begin{aligned} P_n = {} & p_2 p_3 \cdots p_n (1 - p_n)[1 + (p_{n-1} p_{n-2} \cdots p_N)^2 \\ & + (p_{n-1} p_{n-2} \cdots p_{N-1})^2 (1 - p_N)^2 \\ & + (p_{n-1} p_{n-2} \cdots p_{N-2})^2 (1 - p_{N-1})^2 \\ & + \ldots + p_{n-1}^2 (1 - p_{n-2})^2 + (1 - p_{n-1})^2] \end{aligned} \tag{2.12}$$

For the case of partially-stripped projectiles, Taulbjerg (1986) has suggested a correction term to H_{12}. This correction term depends on the quantum numbers n and l of the state into which the transferred electron is captured and is given by

$$f_{nl} = \frac{(-1)^{n-l-1}(2l+1)^{\frac{1}{2}}\Gamma(n)}{[\,\Gamma(n+l+1)\Gamma(n-l)]^{\frac{1}{2}}} \tag{2.13}$$

The coupling matrix element is thus

$$H_{12}^{os} = f_{nl} 9.13\, q^{-\frac{1}{2}} \exp\,[-1.324\, \alpha R_x q^{-\frac{1}{2}}]\ . \tag{2.14}$$

The cross section (σ_n) for capture into a particular final state n is given in terms of the impact parameter b and crossing distance R_x by

$$\sigma_n = 2\pi \int_0^{R_x} P_n b\, db \tag{2.15}$$

where P_n is the probability for capture into the *n*th final state.

Reproduced with permission of the copyright owner. Further reproduction prohibited without permission.

Differential Cross Section

For the collision of highly charged ions with atoms, Coulomb potential curves can be used to predict the differential cross section, $d\sigma/d\Omega$. In the center of mass frame, the scattering angle Θ for classical scattering is given by (Goldstein, 1980):

$$\Theta = \pi - \int_{Path} \frac{b\,|dr|}{r^2\sqrt{(1-\frac{V(r)}{E'}-\frac{b^2}{r^2})}} \qquad (2.16)$$

where b is the impact parameter, V(r) is the scattering potential, r is the internuclear separation and E' is the projectile energy in center of mass frame. From Equation 2.16, by using diabatic Coulomb potential curves, for any impact parameter b, the classical deflection function $\Theta(b)$ in the laboratory frame can be calculated. Since the differential cross section in terms of impact parameter is

$$\frac{d\sigma}{d\Theta} = 2\pi b\,|\frac{db}{d\Theta}| \qquad (2.17)$$

and the differential solid angle in terms of the scattering angle is (Goldstein, 1980)

$$d\Omega = 2\pi \mathrm{Sin}(\Theta)\,d\Theta, \qquad (2.18)$$

then the deflection function of Equation 2.16 can easily be converted to the differential cross section, $d\sigma/d\Omega$.

In order to calculate $d\sigma/d\Omega$, diabatic Coulomb potential curves can be used. We invoke several assumptions: (a) the projectile and target do not interact until the crossing

Reproduced with permission of the copyright owner. Further reproduction prohibited without permission.

point R_x has been reached; (b) after reaching R_x, the reaction proceeds along diabatic curves corresponding to capture on the way in or capture on the way out; (c) the diabatic potential curves used in Equation 2.17, assuming zero interaction in the incoming channel, are obtained from

$$V(r) = \frac{(q-1)}{r} - Q. \tag{2.19}$$

For the simplest model, two state calculation, two different trajectories are possible (way in and way out, see Figure 3). By using the Landau-Zener electron capture probability for each trajectory, p_1 and p_2, the total differential cross section can be written as

$$\frac{d\sigma}{d\Omega} = p_1\left(\frac{d\sigma}{d\Omega}\right)_1 + p_2\left(\frac{d\sigma}{d\Omega}\right)_2 \tag{2.20}$$

where the indices 1 and 2 refer to the two trajectories. Furthermore, this idea can be used for multichannel systems with more than one outgoing channel (see Figure 4). In this case the total semiclassical differential cross section for single-electron capture into a particular final state of the projectile product is

$$\frac{d\sigma}{d\Omega} = \sum_i p_i\left(\frac{d\sigma}{d\Omega}\right)_i. \tag{2.21}$$

Critical and Rainbow Angles

For a two-state case (one entrance and one exit channel), there are two possible paths that the system may follow for electron capture, resulting in a double-branched

Reproduced with permission of the copyright owner. Further reproduction prohibited without permission.

deflection θ(b). The upper branch of the deflection function relates to the projectile trajectory followed by capture on the way in, while the lower branch pertains to the trajectory followed by capture on the way out. The two branches meet at a critical angle θ_c (see Figure 5). This angle corresponds to capture at an impact parameter equal to the crossing radius. Since there is no Coulomb interaction until the projectile travels within the crossing radius, the critical angle is considered a threshold angle for electron capture. For small scattering angles, one can obtain θ_c from Equation 2.16 for b equal to R_x,

$$\theta_c = \frac{Q}{2E_0} \tag{2.22}$$

where Q is the energy gain, and E_0 is the collision energy of the projectile.

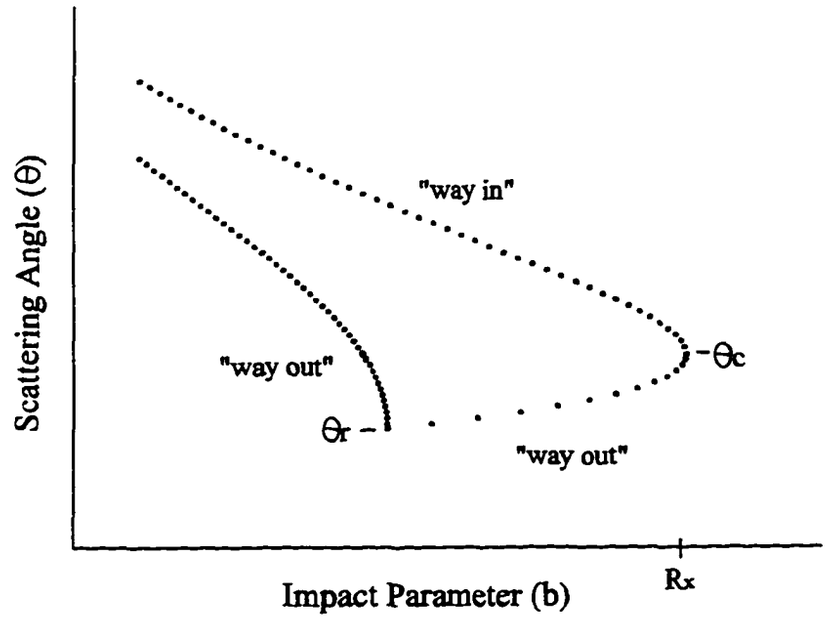

Figure 5. Typical Deflection Function for Two-State Collision Process.

Since there is usually a reaction channel with a higher Q value than the dominant

Reproduced with permission of the copyright owner. Further reproduction prohibited without permission.

exit channel, the entrance channel is not flat but promoted inside the crossing (see Figure 3). This promotion causes the lower branch of the deflection function to rise at small angles, producing a maximum in the differential cross section at a scattering angle Θ_r, i.e. $db/d\Theta \rightarrow \infty$. The angle Θ_r is called rainbow angle that corresponds to the minimum angle for which two impact parameters result in the same scattering angle.

The Reaction Window

The important curve crossings between the diabatic potential energy curves associated with the entrance channel and various exit channels are those which occur at moderate internuclear separations, where the probability for single-electron capture is large. This intermediate range of separations is commonly referred to as the reaction window for the electron capture process. The position of the reaction window for any collision system depends mainly on the collision energy of the projectile. When the collision energy is reduced the adiabaticity at inner crossings becomes increasingly pronounced, while the transition probability at distant crossings becomes larger. Therefore, the reaction window shifts toward larger internuclear separations if the collision energy is reduced and vice versa.

Classical Over Barrier Model

The classical over barrier transition model (COB), originally proposed by Bohr and Lindhard (1954), has been used for a qualitative explanation of the main features of the electron capture process by Ryufuku et al. (1980) and Mann et al. (1981). This model

Reproduced with permission of the copyright owner. Further reproduction prohibited without permission.

describes a projectile ion of effective charge Z_{eff} approaching a target atom and creating a potential barrier.

The electron will be transferred when it has enough energy to overcome the potential barrier between the collision partners. This barrier is given by the superposition of the two Coulomb potentials

$$V(x) = -\frac{Z_{eff}}{x} - \frac{1}{R-x} \tag{2.23}$$

where Z_{eff} is effective charge of incoming ion, R is the internuclear distance and x is the distance measured along the internuclear axis between the target and the projectile (see Figure 6). Electron transfer takes place if two conditions are met. The first condition, from energy conservation, is

$$-I_t - \frac{Z_{eff}}{R} = -\frac{Z_{eff}^2}{2n^2} - \frac{1}{R} \tag{2.24}$$

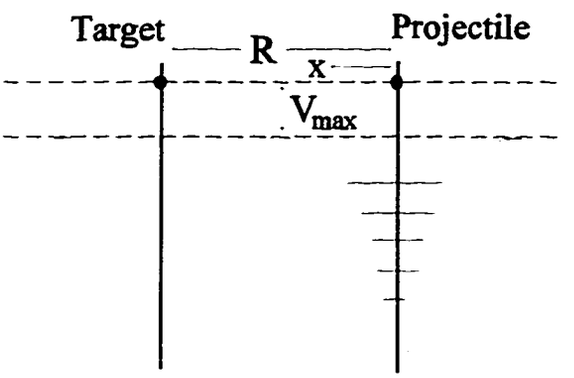

Figure 6. Schematic Representation of Classical Over Barrier Model for Capture Process.

where on the left the first term is the ionization potential of the electron when bound to

Reproduced with permission of the copyright owner. Further reproduction prohibited without permission.

the target atom and the second term is the Coulomb energy due to the projectile ion. while on the right side the first term is the energy of the electron when bound to a level of quantum number n of the projectile and the second term is the Coulomb energy due to the singly-ionized target atom. The second condition for electron transfer is

$$-I_t - \frac{Z_{eff}}{R} \geq V_{max}, \tag{2.25}$$

that is, the energy of the bound electron in the Coulomb field of the projectile ion must be equal to or greater than the maximum barrier height V_{max} between the nuclei. From Equation 2.23, V_{max} can be found by maximizing with respect to x:

$$V_{max} = -\frac{(\sqrt{Z_{eff}}+1)^2}{R} \tag{2.26}$$

One can solve Equations 2.24 - 2.26 to find the critical internuclear distance at which the electron transfer occurs and determine the effective principal quantum number n_c which is populated by the electron capture process (Mann et al., 1981; Ryufuku et al., 1980).

$$R_0 = \frac{Z_{eff}-1}{\frac{Z_{eff}^2}{2n_c^2}-I_t} \tag{2.27}$$

$$n_c \leq \left[\frac{Z_{eff}^2}{2I_t}\left(\frac{2\sqrt{Z_{eff}}+1}{Z_{eff}+2\sqrt{Z_{eff}}}\right)\right]^{\frac{1}{2}} \tag{2.28}$$

Reproduced with permission of the copyright owner. Further reproduction prohibited without permission.

Assuming that the probability for electron capture is 0.5. then the cross section can be calculated using

$$\sigma_o = \frac{1}{2}\Pi R_o^2. \qquad (2.29)$$

Extended Classical Over Barrier Model

The COB model is static and deals with only single-electron capture in low energy ion-atom collisions. Niehaus (1985), by using similar potential barrier used in the COB model, developed an extended classical over barrier (ECOB) model. The ECOB model includes the contributions from capture on the way in and capture on the way out to the calculation of the Q value. In this extended model the binding energy of the *t*th electron in the case of r electron capture with initial ion charge q is

$$E_t = I_t + \frac{q}{R_t^i} - \frac{t+r}{R_t^o} \qquad (2.30)$$

where I_t is the ionization potential of *t*th electron, R_t^i and R_t^o are internuclear distances of *t*th electron for capture on the way in and way on the out, respectively. The energy gain Q is then

$$Q = \sum_{t=1}^{t} (E_t - I_t). \qquad (2.31)$$

Although Q is independent of the collision energy, the model predicts the width of energy gain dynamically, which is proportional to the square root of the collision

Reproduced with permission of the copyright owner. Further reproduction prohibited without permission.

velocity, by using a straight-line trajectories approximation for the nuclei.

Absorbing Sphere Model

In the collision of a multiply charged with atom, the initial channel ($A^{q+} + B$) crosses the product channels ($A^{(q-1)+}+B^{+}$). At these curve crossings strong coupling occurs which leads to electron capture. For sufficiently large charge (q), the number of curve crossings are very large because of the large number of product channels. Assuming unit probability for single-electron capture inside a critical distance R_c, the total cross section simplifies to (Olson et al., 1976)

$$\sigma = \Pi R_c^2 \tag{2.32}$$

Combining Equation 2.6, Equation 2.10, and the condition for obtaining R_c (Olson et al. 1972)

$$0.15 = 2\Pi H_{12}^2(R_c)/\Delta F(R_c)v_o, \tag{2.33}$$

the critical radius R_c for capture is given by expression

$$R_c^2 e^{-2.648\alpha R_c/q^{1/2}} = 2.864 \times 10^{-4} q(q-1)v_0 \tag{2.34}$$

with $\alpha = \sqrt{2I}$, where I_t is the ionization potential of the target atom (in atomic units), and v_0 is the initial velocity of the projectile. Substituting R_c into Equation 2.32 gives the corresponding cross section.

Reproduced with permission of the copyright owner. Further reproduction prohibited without permission.

Muller-Salzborn Scaling Law

Muller and Salzborn (1977) developed an empirical scaling law for electron capture cross sections, from the available experimental cross sections for electron capture of up to 4 electrons in single collisions between multiply charged ions and atoms at collision energies less than 25 keV. The scaling law is in terms of the initial projectile charge q, and the ionization potential of the target I (in eV),

$$\sigma_{q,q-k} = A_k \, q^{\alpha_k} \, I^{\beta_k} \qquad k = 1,\ldots,4 \ , \tag{2.35}$$

where k is number of captured electrons, and A_k, α_k and β_k are fitting parameters. For single-electron capture the parameters are: $A_1 = 1.43 \times 10^{-12}$, $\alpha_1 = 1.17$, $\beta_1 = -2.76$.

Reproduced with permission of the copyright owner. Further reproduction prohibited without permission.

CHAPTER III

EXPERIMENTAL APPARATUS

To study single-electron capture processes involving low-energy multiply-charged ions, a beam of low-energy (30 - 600 eV) multiply charged ions (q=4-8) is directed into an atomic gas target. The ion beam is produced by extracting and charge selecting recoil ions from the interaction region in the recoil ion source, where they are generated in the collision between a target gas and a fast fluorine "pump" beam from the Western Michigan University (WMU) tandem Van de Graaff Accelerator. A differential energy-gain spectrometer is used to characterize the reaction channels produced in the collisions at the collision cell, by measuring the energy-gain of the ion beam following single-electron capture.

In this chapter, the production of the "pump" beam using the WMU Tandem Van de Graaff accelerator and the differential energy-gain spectrometer are described. The present work was performed at the accelerator laboratory at WMU. A schematic diagram of the accelerator facilities is shown in Figure 7.

Pump-Beam Production

A singly charged negative ion beam (in our case F^-) is extracted from the cesium sputter negative ion source (SNICS), with an extraction voltage of 35-50 kV.

Reproduced with permission of the copyright owner. Further reproduction prohibited without permission.

Reproduced with permission of the copyright owner. Further reproduction prohibited without permission.

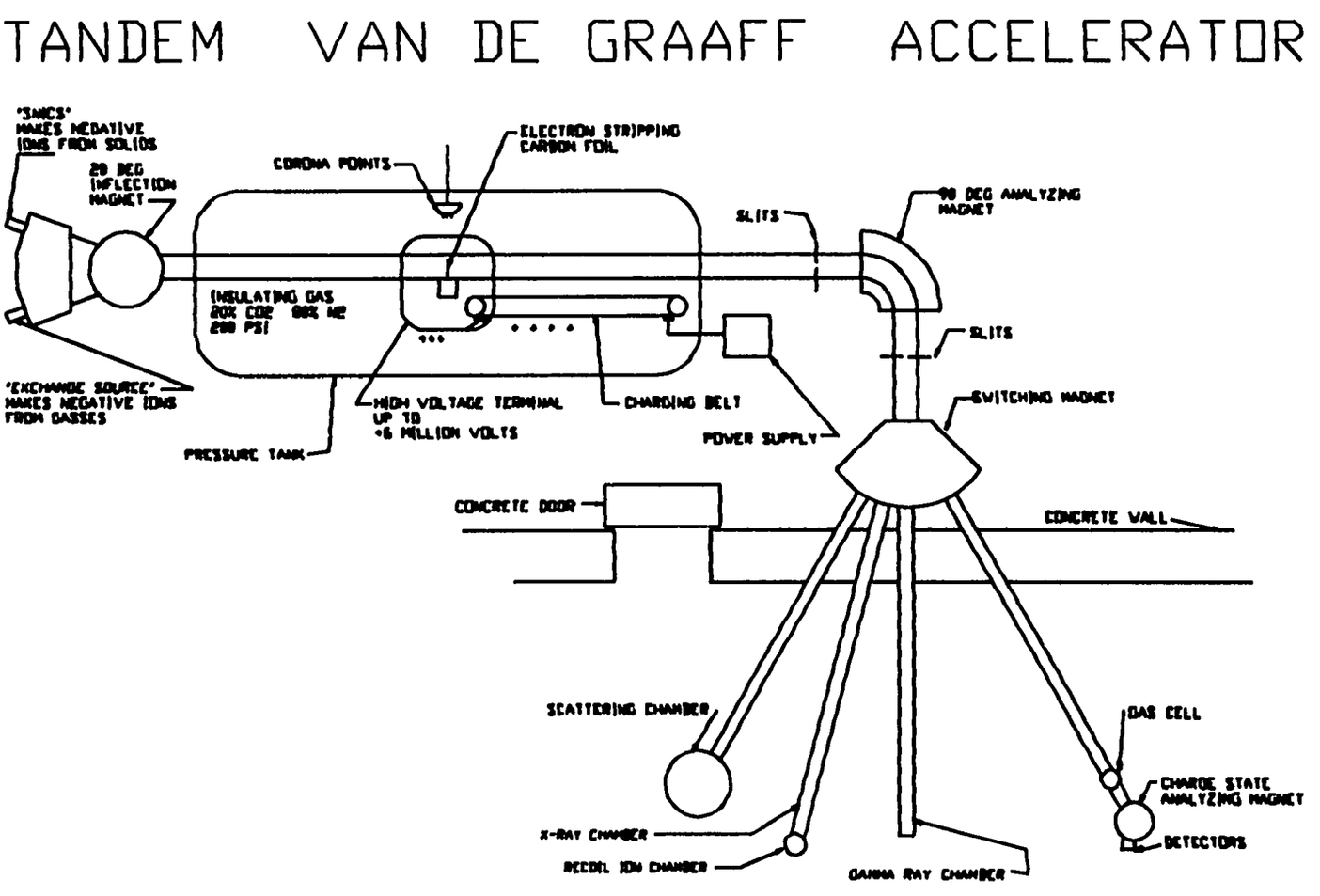

Figure 7. Schematic Diagram of the WMU Tandem Van de Graaff Accelerator.

The beam is analyzed by the 20° inflection magnet, and then injected into the low energy end of the acceleration tube. A positive potential V_t (~ 5MV) is maintained on the terminal halfway inside the accelerator so the ions are accelerated to an energy of eV_t. At the terminal the negative ions are stripped to become positive ions of charge state (+Q) by a low density oxygen gas, and accelerated again away from the terminal. Thus, the final energy of the accelerated ions is (1+Q)eV, when Q is the charge state of ions produced by the stripping process inside the terminal.

The ion beam emerging from the accelerator consists of several charge states of different beam energies which are analyzed by a 90°-analyzing magnet in order to select the desired charge state and energy, (25 MeV F^{4+} ions for this study). The field in the 90°- analyzing magnet is measured by a nuclear magnetic resonance (NMR) technique. The 90°-analyzing magnet focuses the beam on a set of image slits. The portion of the beam striking the image slits produces a current imbalance on the slits due to energy fluctuations in the beam. This current difference between the two image slits can then be fed back to the terminal corona system to stabilize the terminal high voltage. To select among several beam lines set up for different experiments in the target room, a switching magnet is used.

After obtaining a good beam trajectory with a high intensity, the beam is focused by the beam-line quadropole lens by monitoring the beam current at the Faraday cup after the recoil ion source. Typical beam currents collected by the Faraday cup were between 0.5 and 1 μA to optimize the recoil beam current.

Reproduced with permission of the copyright owner. Further reproduction prohibited without permission.

Differential Energy-Gain Spectrometer

A schematic diagram of the differential energy-gain spectrometer used in this work is shown in Figure 8. The apparatus employed a 180° double focusing analyzing magnet, a 90° double focusing electrostatic analyzer with a one-dimensional position sensitive channel-plates detector in the focal plane, and an angular definition before analysis. It is

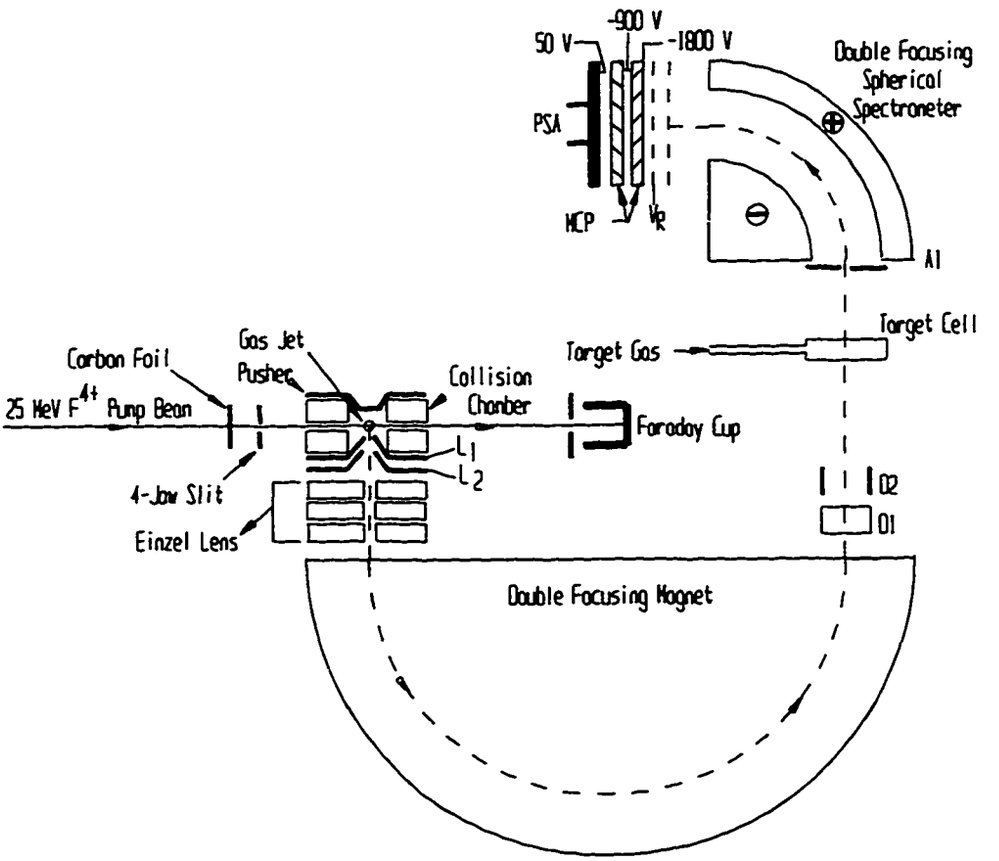

Figure 8. Schematic Diagram of the Experimental Apparatus and the Detector Assembly.

Reproduced with permission of the copyright owner. Further reproduction prohibited without permission.

coupled with a recoil ion source which is pumped by a beam of fast ions from the WMU Tandem Van de Graaff accelerator. The pump beam, a 25 MeV F^{4+} beam in our case. was poststripped to a median charge state of <7+> by using a 10 $\mu g/cm^2$ carbon foil to improve its stripping power, then collimated by a set of four-jaw slits. After collimation. the beam enters the recoil-ion source where highly charged argon ions were produced.

Recoil-Ion Source

The recoil-ion source consists of a collision chamber, a pusher and two lenses (L_1 and L_2). The fast beam passed through the collision chamber, which has entrance and exit apertures of 2.5 and 3 mm diameter, respectively, then collected by a Faraday cup (FC). The gas pressure in the recoil ion source is adjusted until the background pressure in the main chamber increases from ~$3x10^{-6}$ Torr to ~$4x10^{-6}$ Torr. Recoil ions formed in the collision chamber were extracted perpendicular to the pump beam with an acceleration voltage V_{acc}, which is equal to the voltage on the pusher (V_p), through a 2.5 mm diameter aperture in L_1 and 4 mm in L_2, under the influence of a potential field set up by voltages applied to the pusher and lenses L_1 and L_2. In Figure 9 a simulated ion-beam creation in the recoil ion source is shown. A computer simulation program called SIMION is used to calculate the electrostatic fields and beam trajectories for a sample of argon ions accelerated by the pusher at 50 V and focused by the lenses L_1 and L_2 at 49 V and 48 V, respectively. The thin lines in Figure 9 are the equipotential surfaces. The first line from the top shows the potential of 49.95 V and the second line 49.8 V for this sample calculation.

Reproduced with permission of the copyright owner. Further reproduction prohibited without permission.

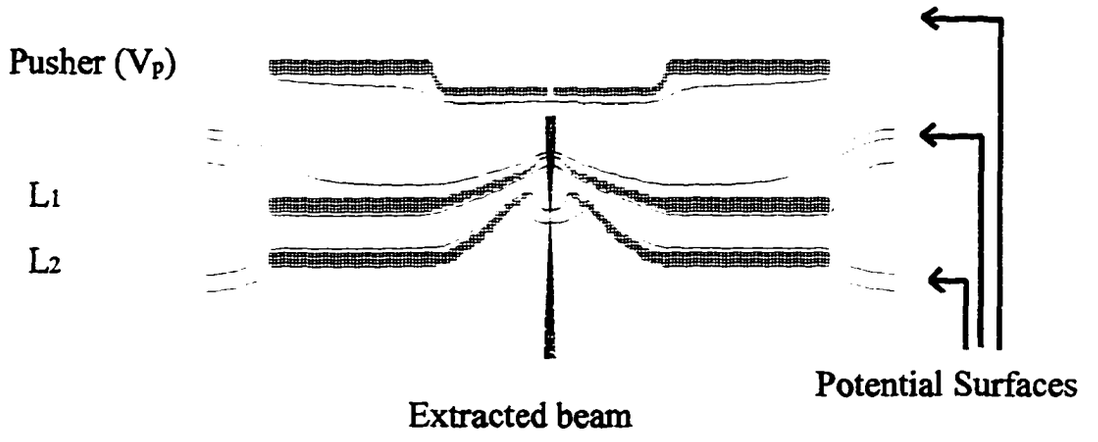

Figure 9. Simulated Ion-Beam Creation in Recoil Ion Source.

Magnetic Charge Spectrometer

After the creation of the argon recoil-ion beam at the desired acceleration voltage, the beam with various charge states was focused by the einzel lens onto the entrance aperture of a 180° double focusing magnetic charge spectrometer, of radius 11.5 cm, to be mass analyzed. For the slits used, the momentum resolution of the magnet is theoretically $\Delta p/p=1.2\%$, but the measured momentum resolution was slightly better.

Following mass analysis, the ion beam was directed with horizantal and vertical deflection plates (D_1 and D_2) toward the 3 mm long collision cell, where collisions with the target atoms takes place. The entrance and the exit apertures of the collision cell were 1 and 2 mm, respectively. The target gas pressure in the cell was sufficiently low to

Reproduced with permission of the copyright owner. Further reproduction prohibited without permission.

ensure single collision conditions. The collision cell pressure was monitored by noting an increase in the background pressure in the main chamber from ~$4x10^{-6}$ Torr to about $5x10^{-6}$ Torr.

Electrostatic Analyzer

Ions scattered through an angle θ into a solid angle of $3x10^{-3}$ sr, which could be selected by means of an aperture A1 (1 mm diameter, see Figure 8) in front of a 90° double-focusing spherical electrostatic analyzer (ESA), were energy analyzed by means of the ESA. The initial energy E of the ion beam of charge q passing through the ESA is given by,

$$E = qV_{acc} = qkV \tag{3.1}$$

where q is the atomic charge, V is the voltage applied to the ESA, and k is the ESA constant given by (Kamber et al., 1987)

$$k = \frac{2R_iR_o}{R_o^2 - R_i^2}, \tag{3.2}$$

where R_o and R_i are radii of the inner and outer electrodes of the ESA. Measured values of the inner and outer radii are 27.6 and 42.4 mm, respectively. Thus k has the theoretical value of 2.26. The experimentally determined value is $k = 2.3 \pm 0.1$ (See Figure 10).

Reproduced with permission of the copyright owner. Further reproduction prohibited without permission.

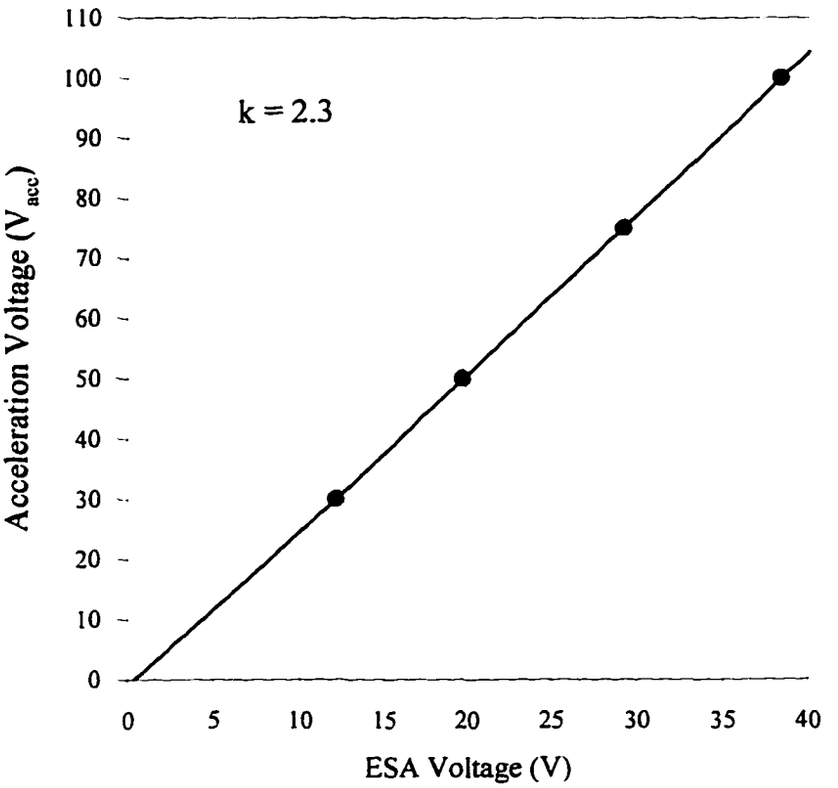

Figure 10. Schematic Diagram Representing the Linear Relationship Between V_{acc} and ESA Voltage (V). The Slope of This Curve is Equal to the Analyzer Constant k.

Position Sensitive Detector

The analyzed ions were then detected by a one-dimensional position-sensitive microchannel plate detector, which is located at the focal plane of the ESA. The detector device consists of two 2.5 cm diameter microchannel plates (MCP), and a one-dimensional position-sensitive anode encoder (PSA). The voltage applied across the entire configuration was about -1800 V, thus the potential across each plate was about

Reproduced with permission of the copyright owner. Further reproduction prohibited without permission.

-900 V . When an ion strikes the front channel plate the resulting electron cascade from the two microchannel plates was accelerated towards and collected by the anode. The fraction of charge collected on electrodes located at each side of the anode is inversely proportional to the distance from the electrode to where the electrons hit the anode. The relative position of the ions striking the MCP is then determined by the ratio between the resulting voltage pulse at one electrode and the sum of the voltage pulses of the two electrodes, that is

$$X = \frac{V_U}{(V_U + V_L)} \tag{3.3}$$

where X is the relative position along the active dimension, and V_U and V_L are the voltage pulse heights at the upper and lower electrodes, respectively.

Electronics

Data were collected using the electronics setup shown schematically in Figure 11. Signals from each electrode of the position sensitive anode (PSA) were first identically amplified by using preamplifiers (Ortec model 109A) and spectroscopy amplifiers (AMP, Ortec model 451) and then summed using a dual sum/invert amplifier (DSI, Tennelec model TC253). The signal then passed to the position sensitive detector analyzer (PSD, Ortec model 466) where the voltage signals were divided, producing a voltage signal whose height is proportional to the location of the incident ion's position on the PSA. The analog signals of the position output of the PSD were directed to an analog-to-digital

Reproduced with permission of the copyright owner. Further reproduction prohibited without permission.

converter (ADC) which was gated by the counter timer, preset for some maximum number of counts of integrated fast beam current accumulated bye the Faraday cup. The pulse rate of the output signal (energy output of the PSA) was measured using a ratemeter (RM, Ortec mo-del 744). Digital position signals from the ADC go to the input module of the CAMAC crate.

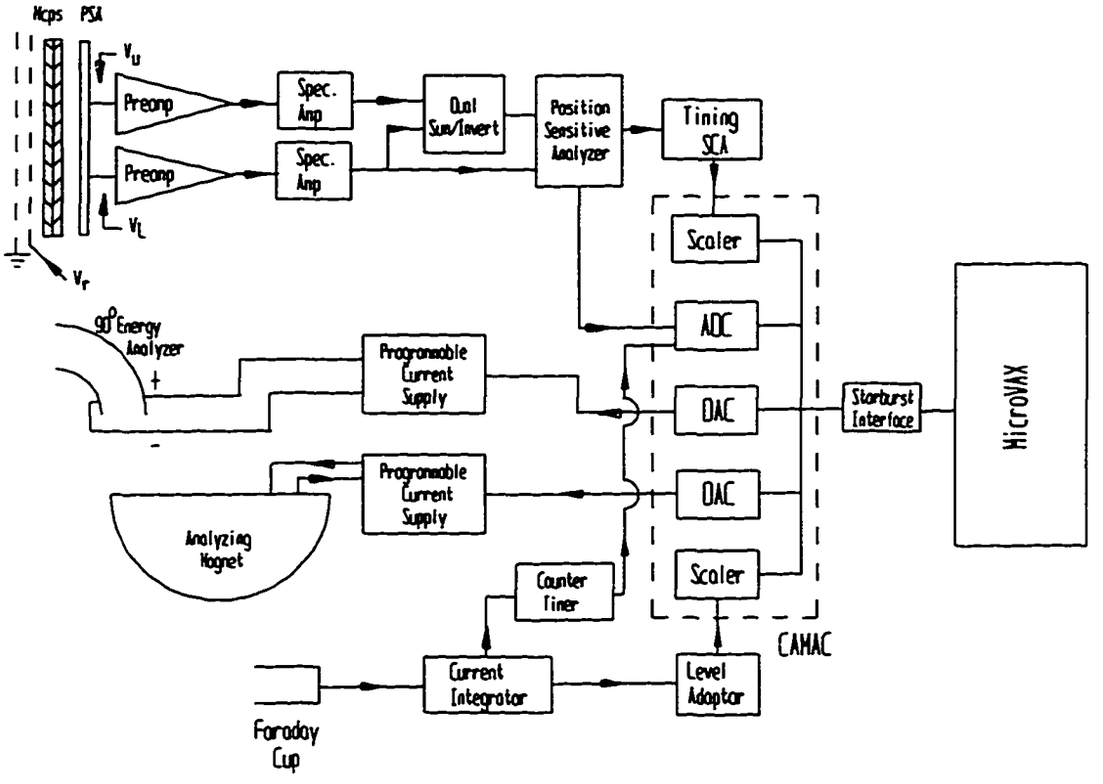

Figure 11. Electronics Block Diagram for the Energy-Gain Spectrometer.

A STARBURST interface module was used to transfer data to a MicroVAX computer system enabling conversion from position distribution information to energy distribution information.

Reproduced with permission of the copyright owner. Further reproduction prohibited without permission.

CHAPTER IV

DATA ANALYSIS

The data collected from the experimental apparatus are analyzed to obtain charge state spectra for the recoil ions produced in the recoil ion source and the energy-gain spectra for single-electron capture by selected projectile (recoil) ions. The energy-gain spectra are then analyzed for the following information; the final state population following single-electron capture (SEC), differential cross sections, and total cross sections.

Charge-State Spectroscopy

A charge-state spectrum of argon recoil ions produced in the recoil-ion source was obtained by varying the magnet current of the 180°-double focusing magnet and the ESA voltage was kept fixed. Figure 12 shows the relative abundance of recoil argon ions of various charge states for 25 MeV F^{4+} incident on Ar. To identify the charge state of each peak, the square root of the mass-to-charge ratio of the recoil ion peaks as a function of the 180°-double focusing magnet current was plotted (see Figure 13). The linearity of this plot gives the confirmation of the correct identification of the peaks. The nitrogen ion (N^+) peak seen in the spectrum in Figure 12 arises from the presence of nitrogen as an impurity.

Reproduced with permission of the copyright owner. Further reproduction prohibited without permission.

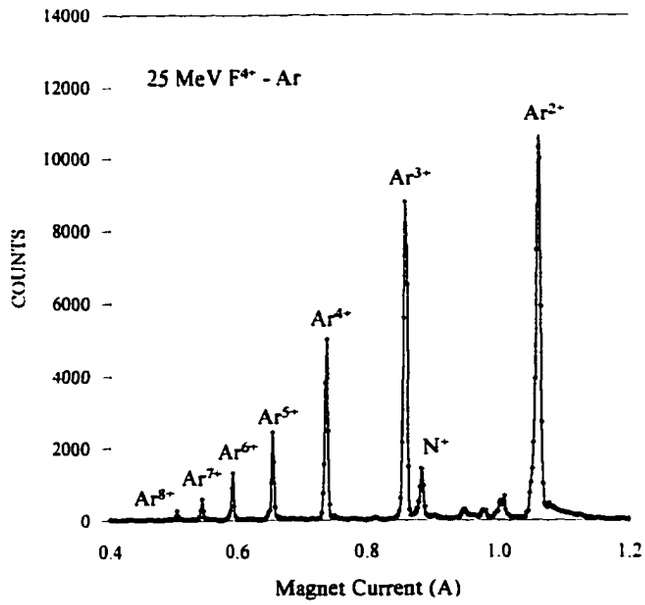

Figure 12. Charge-State Select Spectrum for Ar Recoil Ions Produced in the Recoil-Ion Source.

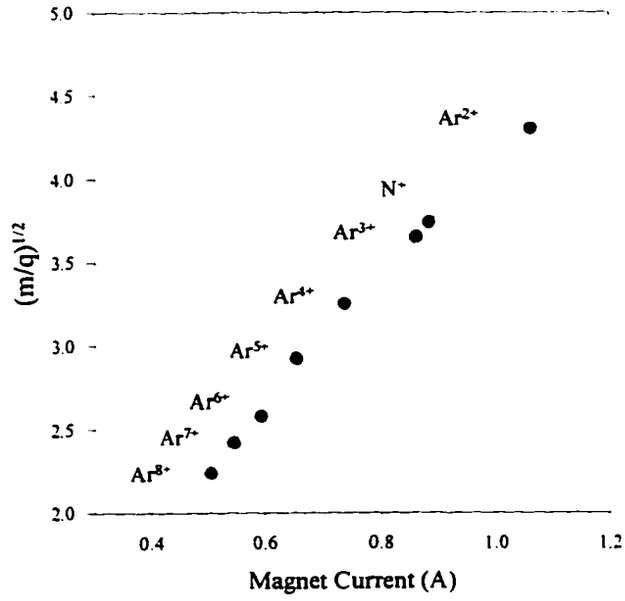

Figure 13. Square Root of the Mass-to-Charge Ratio of the Recoil Ar Ions vs Magnet Current.

Reproduced with permission of the copyright owner. Further reproduction prohibited without permission.

Translational Energy-Gain Spectra

The energy gain (Q) of the projectile following single-electron capture in terms of the acceleration voltage (V_{acc}) and the voltage applied across the plates of the ESA is given by

$$Q = \left[\left(\frac{q'V}{qV_o}\right) - 1\right]V_{acc}q \qquad (4.1)$$

where q and q' are the atomic charges of the projectile before and after the collision, respectively, and V_0 and V are the applied voltages to the ESA for which the primary beam and the product ions (i.e. charge-changed projectile) are passed (Kamber et al., 1987).

In order to calculate the energy gained by the projectile ion during a collision, a position calibration had to be performed. The detector was calibrated by positioning the direct beam at different locations and by varying the applied voltage to the ESA. Plotting the channel number versus the applied voltage produced a line whose slope, the channel number per voltage, allowed for conversion from channel numbers to voltages (see Figure 14). Energy-gain spectra were then revealed by converting the ESA voltage to the Q-value using Equation 4.1. The projectile outgoing reaction channels following single-electron capture are listed in Tables 1- 3. The ionic energy levels used in preparing the tables were taken from Moore (1970) and Bashkin and Stoner (1978). These tables were used to determine which outgoing reaction channels are observed in the collision systems

Reproduced with permission of the copyright owner. Further reproduction prohibited without permission.

studied in this work by comparing the energy-gain spectra with theoretical Q-values using Equation 2.2 and 2.4. The Q-value corresponding to each of the observed states is represented by a vertical line in the energy-gain spectrum.

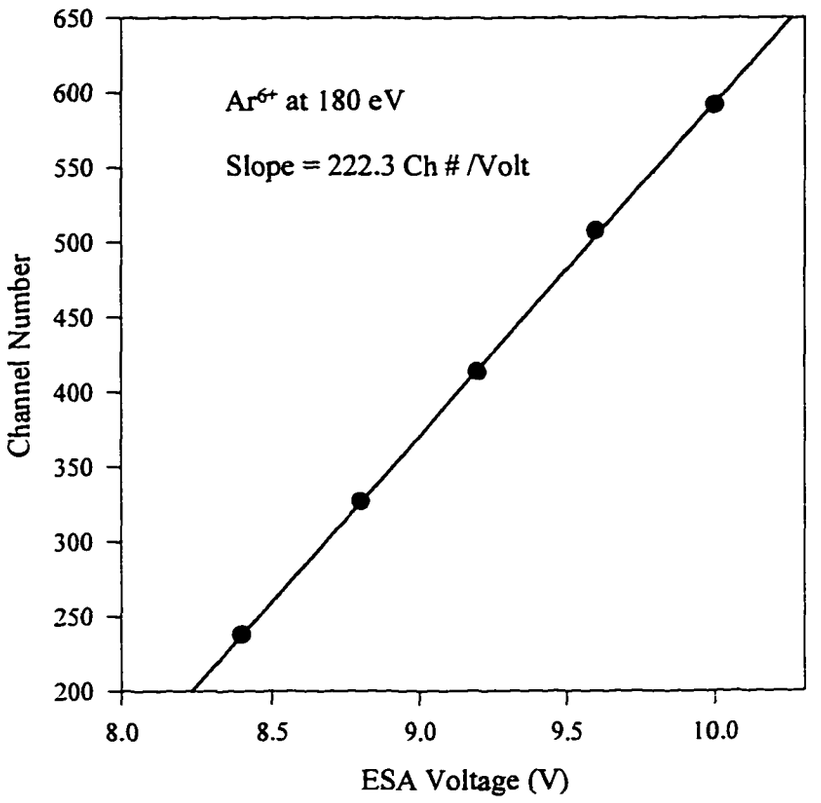

Figure 14. Position of the Projectile Peaks as a Function of the ESA Voltages.

The errors in the measured Q-values are mainly due to the least-squares fit to the position calibration curve, the channel number versus the ESA voltages, and the stability of the voltage applied to the ESA. Under these conditions errors in the energy-gain scale were less than ±1 eV.

The measured energy resolution ($\Delta E/E_o$) of the direct beam ranged from 0.85 to

Reproduced with permission of the copyright owner. Further reproduction prohibited without permission.

Table 1

ΔE Values and Projectile Products for Single-Electron Capture in Ar^{4+} ($3p^2\ ^3P$) - Ne Collisions

Projectile Product	Energy Defect ΔE (eV)
Ar^{3+} ($3s^2\ 3p^3\ ^2D$)	38.23
Ar^{3+} ($3s^2\ 3p^3\ ^2P$)	33.91
Ar^{3+} ($3s\ 3p^4\ (^3P)\ ^4P$)	23.54
Ar^{3+} ($3s\ 3p^4\ (^1D)\ ^2D$)	20.23
Ar^{3+} ($3s\ 3p^4\ (^3P)\ ^2P$)	17.6
Ar^{3+} ($3s\ 3p^4\ (^1S)\ ^2S$)	16.18
Ar^{3+} ($3s\ 3p^2\ (^3P)\ 3d\ ^2P$)	17.6
Ar^{3+} ($3p^2\ (^3P)\ 3d\ ^4F$)	15.83
Ar^{3+} ($3p^2\ (^3P)\ 3d\ ^4D$)	15.01
Ar^{3+} ($3p^2\ (^3P)\ 3d\ ^4P$)	10.86
Ar^{3+} ($3p^2\ (^3P)\ 3d\ ^2D$)	10.37
Ar^{3+} ($3p^2\ (^3P)\ 3d\ ^2F$)	7.66
Ar^{3+} ($3p^2\ (^1D)\ 3d\ ^2F$)	15.12
Ar^{3+} ($3p^2\ (^1D)\ 3d\ ^2G$)	12.47
Ar^{3+} ($3p^2\ (^1D)\ 3d\ ^2D$)	8.64
Ar^{3+} ($3p^2\ (^3P)\ 4s\ ^4P$)	7.21
Ar^{3+} ($3p^2\ (^3P)\ 4s\ ^2P$)	7.1
Ar^{3+} ($3p^2\ (^1D)\ 4s\ ^2D$)	6.48
Ar^{3+} ($3p^2\ (^1S)\ 4s\ ^2D$)	5.83

Source: Bashkin, S., & Stoner, J.O. (1978). Atomic energy levels and Grotrian Diagrams (Amsterdam: North-Holland, 239-241).

Reproduced with permission of the copyright owner. Further reproduction prohibited without permission.

Tabel 2

ΔE Values and Projectile Products for Single-Electron Capture in $Ar^{5+}(3s^2\ 3p\ ^2P)$ - Ne Collisions

Projectile product	Energy Defect ΔE (eV)
Ar^{4+} $(3s^2\ 3p\ (^2P)\ 3d\ ^1P)$	22.19
Ar^{4+} $(3s^2\ 3p\ (^2P)\ 4s\ ^3P)$	16.52
Ar^{4+} $(3s^2\ 3p\ (^2P)\ 4s\ ^1P)$	16.11
Ar^{4+} $(3s^2\ 3p\ 4p\ ^1P)$	11.83
Ar^{4+} $(3s^2\ 3p\ 4p\ ^3D)$	11.52
Ar^{4+} $(3s^2\ 3p\ 4p\ ^3S)$	10.80
Ar^{4+} $(3s^2\ 3p\ 4p\ ^3P)$	10.76
Ar^{4+} $(3s^2\ 3p\ 4p\ ^1D)$	9.83
Ar^{4+} $(3s^2\ 3p\ 4p\ ^1S)$	8.63

Source: Bashkin, S., & Stoner, J.O. (1978). Atomic energy levels and Grotrian Diagrams (Amsterdam: North-Holland, 243-245).

1.2 %, where ΔE is the full width at half maximum (FWHM) of the energy distribution of the direct beam and E_o is projectile energy at which the analyzer is tuned. The energy resolution of the ESA for a 600 eV Ar^{6+} ion beam was found to be 1.17%, as shown in Figure 15.

Differential Cross Sections

The differential cross sections ($d\sigma/d\Omega$) were found by calculating the area under

Reproduced with permission of the copyright owner. Further reproduction prohibited without permission.

Table 3

ΔE Values and Projectile Products for Single-Electron Capture in Ar^{6+} ($3s^2\ ^1S$) - He and Ne Collisions

Projectile Product	Energy Defect (eV)	
	He	Ne
$Ar^{5+}(3s^2\ 4s)$	23.98	27.0
$Ar^{5+}(3s\ 3p\ (^3P)\ 3d\ ^2F)$	23.74	26.76
$Ar^{5+}(3s\ 3p\ (^3P)\ 3d\ ^2P)$	19,85	22.87
$Ar^{5+}(3s\ 3p\ (^1P)\ 3d\ ^2F)$	19.76	22.78
$Ar^{5+}(3s\ 3p\ (^1P)\ 3d\ ^2D)$	17.38	20.4
$Ar^{5+}(3s^2\ 4p\ ^2P)$	17.43	20.45
$Ar^{5+}(3s^2\ 4d\ ^2D)$	10.04	13.06
$Ar^{5+}(3s^2\ 4f\ ^2P)$	6.26	9.28

Source: Bashkin, S., & Stoner, J.O. (1978). Atomic energy levels and Grotrian Diagrams (Amsterdam: North-Holland, 247-249).

the peaks in the energy-gain spectrum at different scattering angles, using a curve fitting program, called MEWA, after normalizing each spectrum to the total amount of the pump beam charge collected at the Faraday Cup.

Total Cross Sections

In order to measure the total cross sections for single-electron capture by multiply charged argon ions from He and Ne atoms, we removed aperture A1, which was located in front of the ESA (see Figure 6, in Chapter III). This provides an angular acceptance

Reproduced with permission of the copyright owner. Further reproduction prohibited without permission.

of almost ±10°.

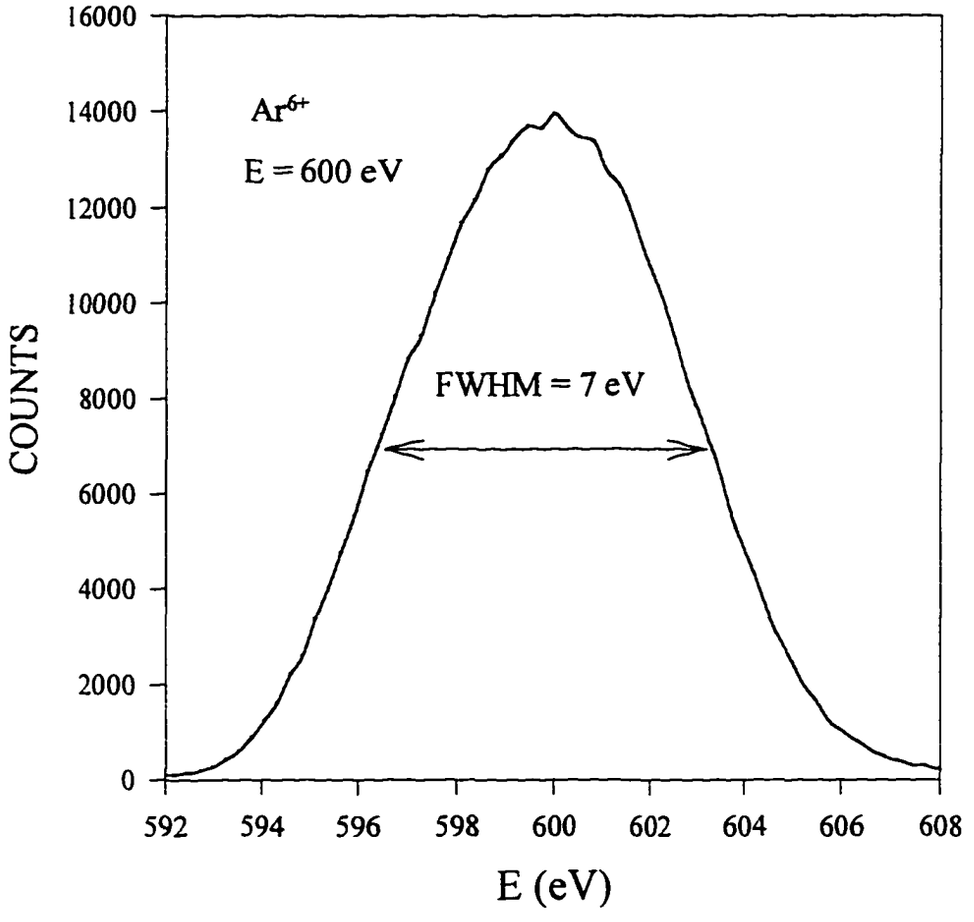

Figure 15. Energy Resolution of the ESA. The Full Width at Half Maximum (FWHM) is 7 eV for 600 eV Ar^{6+} Recoil Source.

To find the total cross sections, the relative intensities, I/I_o, where I is the number of incoming Ar^{q+} ions in an unit time and I_o is the number of $Ar^{(q-1)+}$ ions produced in the normalizing to the total amount of pump beam charge collected at the Faraday Cup. The same time interval, were measured as a function of the collision gas pressure after results

Reproduced with permission of the copyright owner. Further reproduction prohibited without permission.

for 300 eV Ar^{6+} - Ne collisions are shown in Figure 16, indicating linear dependence on pressure difference up to 1.5×10^{-3} Torr. The total cross section (σ) was calculated using the relationship

$$\sigma = \frac{I/I_o}{nL}, \tag{4.2}$$

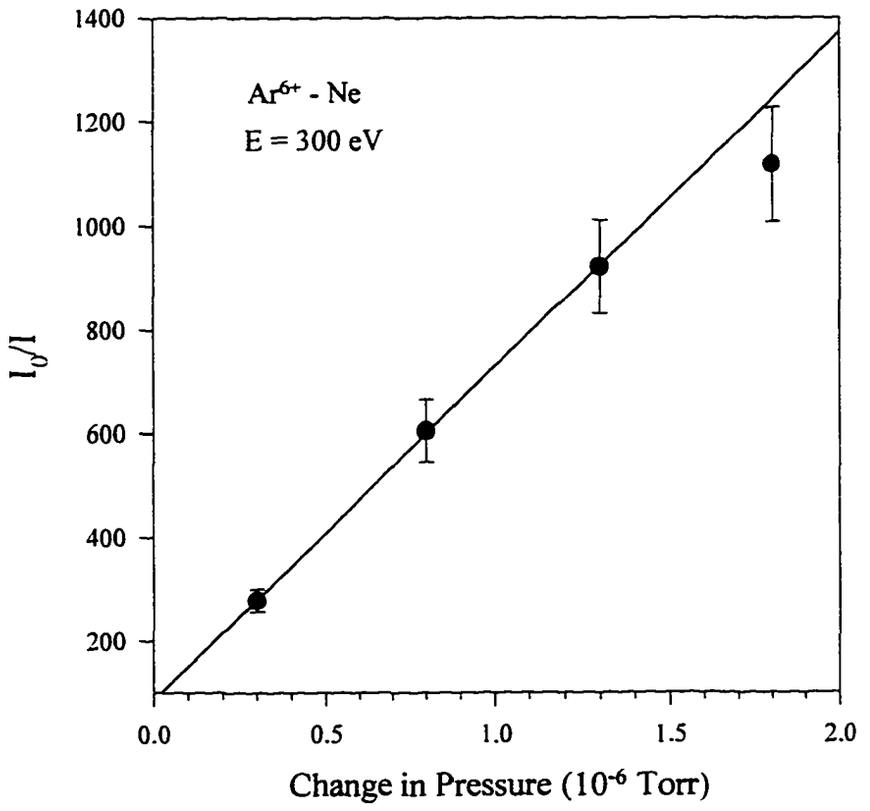

Figure 16. Relative Cross Section for Single-Electron Capture in the Ar^{6+} - Ne Collision at 300 eV Collision Energy.

Reproduced with permission of the copyright owner. Further reproduction prohibited without permission.

where n is the number of target atoms per unit volume in the collision cell and L (=3 mm) is the length of the cell. The absolute scales for the cross sections were evaluated by normalizing the results of this study to the total capture cross section measurements of Justiniano et al. (1989). The absolute uncertainty is estimated to be ±30 %, including the20 % evaluated by Justiniano for their values of the total cross section.

Reproduced with permission of the copyright owner. Further reproduction prohibited without permission.

CHAPTER V

RESULTS AND DISCUSSION

In this chapter the translational energy-gain spectra, differential cross sections, and total cross sections for single-electron capture by Ar^{q+} ions from He and Ne atoms are presented. However, for the following reasons we have studied in more detail only the doubly differential (in energy-gain and projectile scattering angle) cross sections for collisions of Ar^{q+} ions (q = 4 - 6) with Ne and Ar^{6+} ions with He at collision energies between 15 and 100 qeV and scattering angles between 0° and 8°. First, Yaltkaya et al. (1993) have previously discussed the energy-gain spectra and differential cross sections for single-electron capture by Ar^{q+} ions (q = 4, 5) from He and Ar. Second, because of the limited space one or two collision energies for each collision system were chosen. Finally, the translational energy-gain spectra presented here were selected due to their high statistics. In the following sections, the experimental results and a discussion of the individual collision system are presented and classified according to the measurements of translational energy-gain spectra, differential cross sections, and total cross sections for single-electron capture.

Reproduced with permission of the copyright owner. Further reproduction prohibited without permission.

Translational Energy-Gain Spectra

Ar^{4+} - Ne Collisions

Figure 17 shows the translational energy-gain spectra for the formation of Ar^{3+} ions from the reaction of the 120 eV Ar^{4+} ions with Ne at different projectile laboratory scattering angles. The observed collision spectrum at 0° scattering angle is dominated by a peak due to capture from the ground state Ar^{4+} ($3p^2\ ^3P$) ions into the 3d ^2D and ^4P excited states of the Ar^{3+} product ions, with contributions from capture accompanied by the excitation of the target product via the reaction channel

$$Ar^{4+}(3p^2\ ^3P) + Ne\ (2p^6\ ^1S) \rightarrow Ar^{3+}(3p^3\ ^4S) + Ne^{+}(2p^6\ ^2S) + 11.3\ eV. \qquad (5.1)$$

The broad peak, centered around Q = 14.5 eV, is due to capture into the 3d ^4D and ^4F states of Ar^{3+}, with contributions due to transfer excitation into the $3p^4\ ^2S$ and ^2P and $3p^2\ (^1D)3d\ ^2F$ states of Ar^{3+}. This peak is also energetically identifiable with capture from the low-lying metastable states $3p^2\ ^1D$ and ^1S of the Ar^{4+} ion into the $3p^2\ (^1D)3d\ ^2G$ and 3d ^2D states of Ar^{3+}, respectively. However, there can also be contributions from capture into the $3p^3\ ^4S$ state of Ar^{3+} accompanied by excitation of the target product into the $2p^6\ ^2S$ state of Ne^{+}, which it strongly overlaps within the same range of the Q-value. The unresolved structure at about Q ≤ 9 eV is due to capture into the 3d ^2F, $3p^2\ (^1D)3d\ ^2D$ and 4s ^4P states of Ar^{3+}.

As the scattering angle is increased, single-electron capture into the 3d state of Ar^{3+} remains dominant, but the reaction channels correlated with capture into the 3d ^4D

Reproduced with permission of the copyright owner. Further reproduction prohibited without permission.

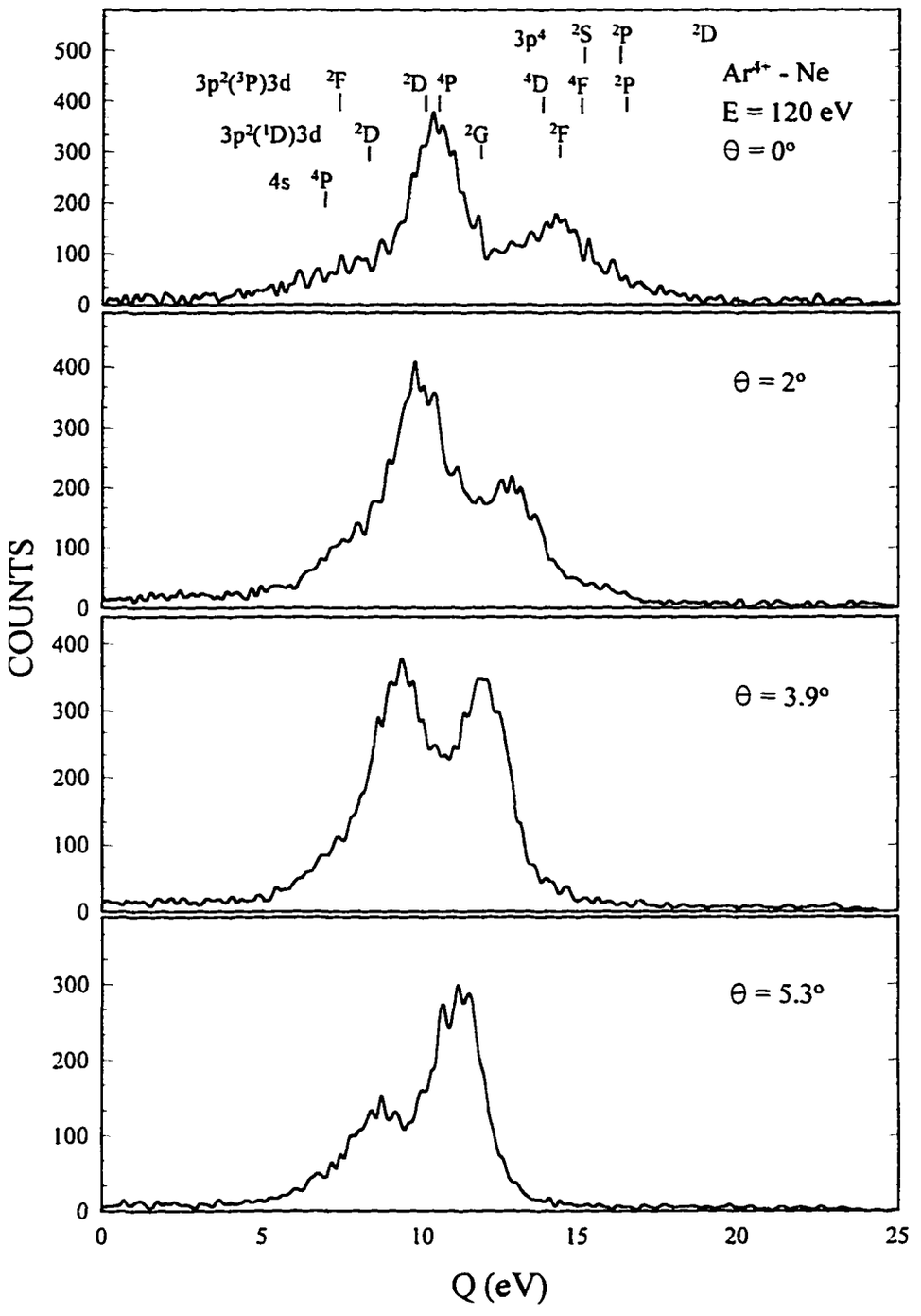

Figure 17. Translational Energy-Gain Spectra for Single-Electron Capture by 120 eV Ar^{4+} Ions From Ne at Different Projectile Laboratory Scattering Angles.

Reproduced with permission of the copyright owner. Further reproduction prohibited without permission.

and ^4F, $3p^2$ (^1D)3d ^2F states, and the presence of metastable states ($3p^2$ ^1D and ^1S) in the Ar^{4+} ion beam become more pronounced relative to the dominant peak. In addition, a relative shift of about 2 eV in energy gain of the 3d ^4P channel is observed in going from a scattering angle of 0° to 5.3°. This is attributed to the translational energy given to the target, and is in accordance with energy and momentum conservation rules.

At an impact energy of 200 eV (see Figure 18), the zero-angle spectrum shows that the relative cross section for the capture into the 3d state is equivalent to that due to capture from the metastable state ($3p^2$ ^1D) of Ar^{4+} into the $3p^2$(^1D)3d ^2G state. There are also contributions from the reaction channel involving the formation of Ar^{3+}($3p^3$ ^4S) due to capture from the incident metastable state of Ar^{4+} ($3p^2$ ^1D), accompanied by excitation of the target product. As the scattering angle is increased, the latter process remains dominant, while the relative importance of capture into the 3d state of Ar^{3+} is strongly decreased. This indicates that the angular distribution for capture into the 3d state is strongly peaked in the forward direction in the Ar^{4+} - Ne collisions. In addition, another particularly interesting feature of the scattering angle dependence of single-electron capture spectra is that, with increasing scattering angles, contributions from avoided crossings at smaller internuclear separations (large Q-value), become gradually more important as one would expect. In general, at the forward scattering or smaller angles, the larger impact parameter collisions play an important role in the electron capture process since the avoided crossings at small internuclear separation (large Q-value) cannot be reached, and make no contribution. As the angle is increased, contributions from successively smaller internuclear separation regions appear.

Reproduced with permission of the copyright owner. Further reproduction prohibited without permission.

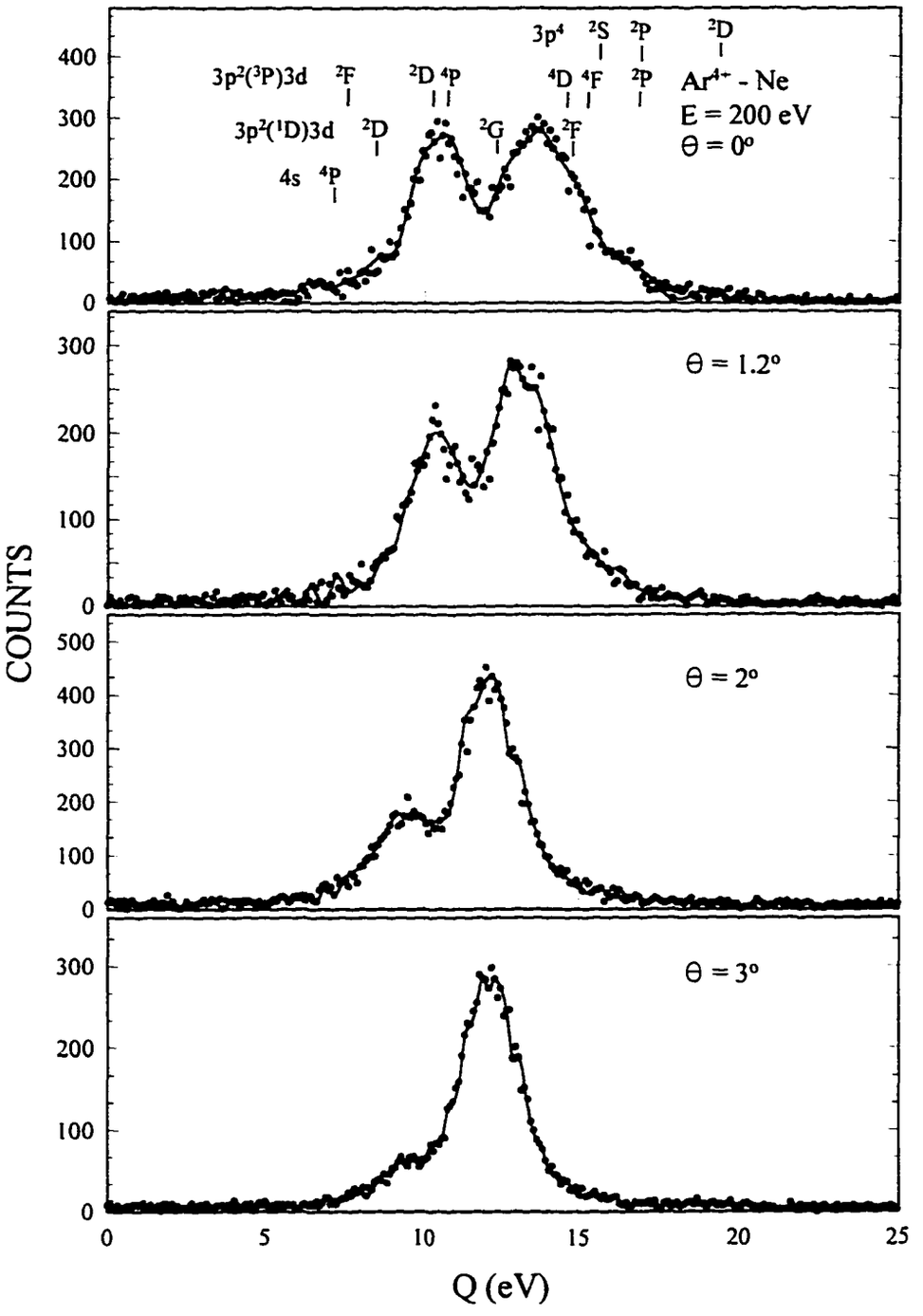

Figure 18. Translational Energy-Gain Spectra for Single-Electron Capture by 200 eV Ar^{4+} Ions From Ne at Different Projectile Laboratory Scattering Angles.

Reproduced with permission of the copyright owner. Further reproduction prohibited without permission.

In their measurements at 8 keV and 12 keV, respectively, Lee et al. (1995) and Kamber (1988) found that the dominant reaction channel is due to capture from the ground state of $Ar^{4+}(3p^2\ ^3P)$ into the $3s3p^4\ ^2S$ state of Ar^{3+} at a Q-value of 16.2 eV. This is attributed to the high collision energy they used since the position of the reaction window, the and range of Q values where the probability for single-electron capture is large, depends mostly on the collision energy of the projectile. When the collision energy is reduced, the adiabaticity of inner crossings will become increasingly pronounced, while the transition probability at distant crossings becomes larger. Therefore the reaction window shifts towards larger internuclear separations (small Q-value) if the collision energy is reduced, and vice versa. Lee et al. (1995) also observed, in addition to the eight identifiable peaks, a peak at Q = 14.9 eV, which is correlated with the presence of a long-lived quintet-state of Ar^{4+} $(3s3p^3\ ^5S)$ in the ion beam, at about 7.5 eV above the ground state.

Figure 19 shows the translational energy-gain spectra observed for the formation of Ar^{3+} from the reaction of Ar^{4+} with Ne at 0° scattering angle and different collision energies. As the collision energy is increased, single-electron capture into the 3d state of Ar^{3+} remains dominant, but the relative importance of the reaction channels due to the presence of metastable states in the Ar^{4+} incident beam significantly increases and becomes the dominant process at an impact energy of E = 300 eV. This can be qualitatively understood from concepts of the reaction window as discussed above.

Figure 19 also shows our calculated reaction windows, using both a single-crossing Landau-Zener (LZ) model (Landau, 1932; Zener, 1932; Olson, 1976) and the

Reproduced with permission of the copyright owner. Further reproduction prohibited without permission.

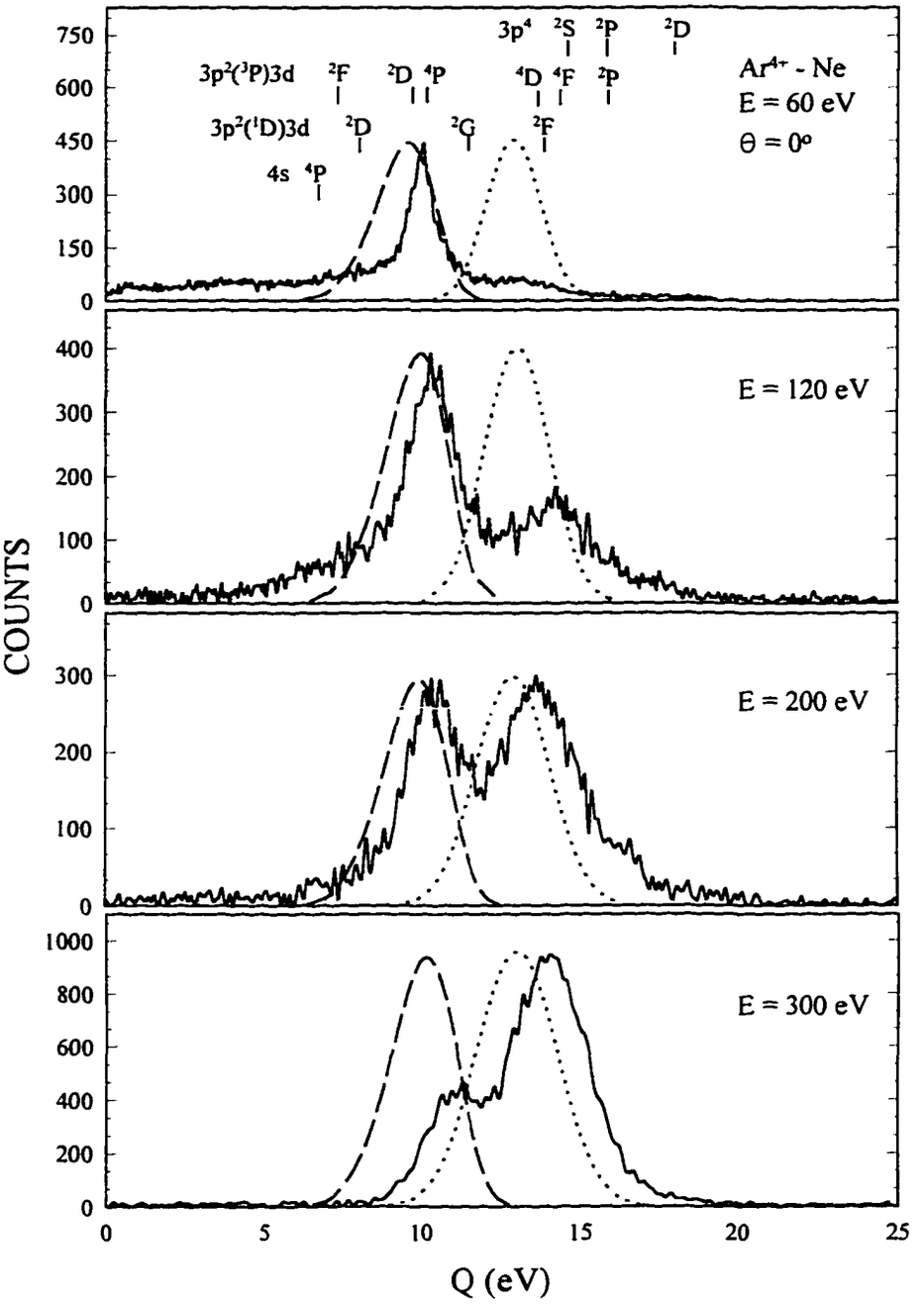

Figure 19. Translational Energy-Gain Spectra for Single-Electron Capture by Ar^{4+} Ions From Ne at Different Collision Energies. Also Shown are Reaction Windows Calculated on the Basis of a Single-Crossing LZ Model (Dashed Curve) and the ECOB Model (Dotted Curve).

Reproduced with permission of the copyright owner. Further reproduction prohibited without permission.

extended version of the classical over-the-barrier (ECOB) model (Niehaus, 1986). Calculated peak values have been normalized to our observed peak values in the translational energy-gain spectrum. The reaction window based on the ECOB model is assumed to be Gaussian around the classical value of the minimum-Q value [$Q = (q-1)/R_c$], which is related to the time dependence of the potential barrier height, with a width proportional to $v^{1/2}$, where v is the impact velocity of the projectile ions. The reaction window based on a single-crossing LZ model, using the Taulbjerg expression for the coupling matrix H_{12} with Taulbjerg factor f_{nl} (3d) = 0.408 (Taulbjerg, 1986), predicts the 3d channel to be the dominant process at low energies. The reaction window based on the ECOB model accommodates the 3d ^4D, ^4F, $3p^2$ (^1D)3d ^2F, and $3p^4$ channels and favors larger Q values compared to the dominant channel.

Ar^{5+} - Ne Collisions

Figure 20 shows the translational energy-gain spectra of the product Ar^{4+} ions in the Ar^{5+} - Ne collisions at an impact energy of 250 eV and different projectile laboratory scattering angles. At 0° scattering angle, two peaks are clearly resolved. The stronger peak correlates with capture from the ground state of the incident Ar^{5+}($3p\ ^2P$) ion into the 4p states of Ar^{4+}. The smaller peak arises from capture into the 4s states of Ar^{4+}, with a contribution from the transfer ionization process. No data on state-selective single-electron captureby low-energy Ar^{5+} ions from Ne are, however, available for comparison. Again, comparison with the results of Kamber (1988) at 15 keV shows that capture into the 4s state shows a larger contribution in his measurements, which is due

Reproduced with permission of the copyright owner. Further reproduction prohibited without permission.

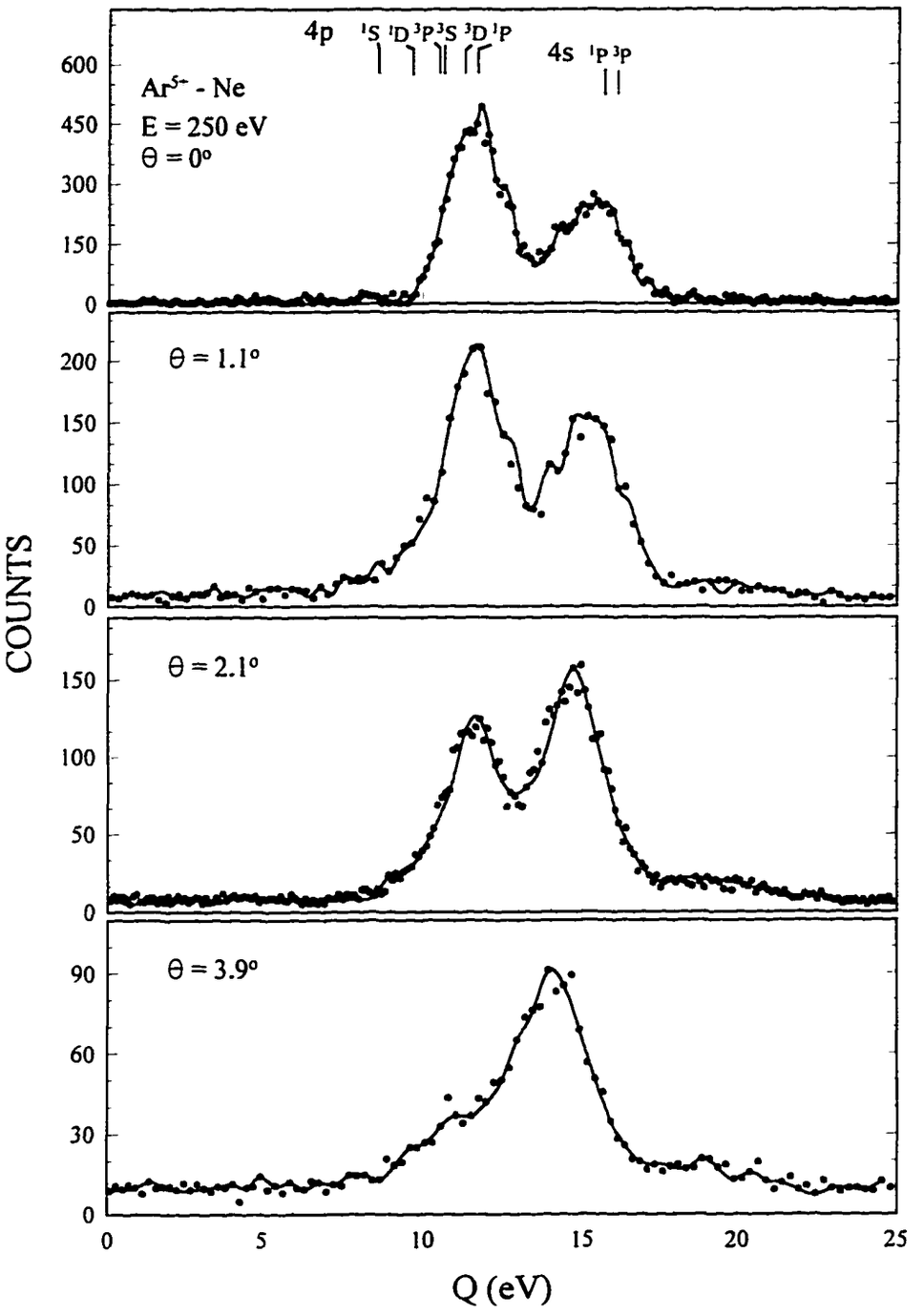

Figure 20. Translational Energy-Gain Spectra for Single-Electron Capture by 250 eV Ar^{5+} Ions From Ne at Different Projectile Laboratory Scattering Angles.

Reproduced with permission of the copyright owner. Further reproduction prohibited without permission.

to the high collision energy he used. Cavalcanti et al. (1996) have determined the five energy levels of the $3p^4$ configuration of Ar^{4+} from the observed wavelengths by an iterative optimization procedure in which the individual wavelengths are weighted according to their uncertainties. The Q-values for capture into the $3p^4$ ^3P, ^1D and ^1S states of Ar^{4+} are 20.64, 18.94 and 13.14 eV, respectively.

As the scattering angle increases the importance of the single-electron capture in 4s states of Ar^{4+} increases, whereas the relative importance of capture into the 4p state is strongly decreased. In greater detail, Figure 21 shows the probabilities for single-electron capture into the 4p and 4s states taken from the observed spectra as function of the scattering angle for impact energies of 150 and 250 eV. The electron capture probability is found from the ratio of the area under each reaction channel to the total area, i.e., $P_{nl} = \sigma_{nl}/\sigma_{total}$. The areas under each channel were determined by fitting Gaussian peak shapes of fixed position and widths to the measured spectra. For impact energy of E = 150 eV the 4p channel is dominant not only at small scattering angles but over the angular range $0 \leq \theta \leq 4.6°$. For E = 250 eV, the 4p channel is still dominant at small angles ($\theta \leq 1.6°$), but for $\theta \geq 1.8°$ the 4s channel prevails.

The variation of the translational energy spectra for single-electron capture processes as a function of collision energy for the Ar^{5+} - Ne collision system is illustrated in Figure 22. It should be noted that the relative importance of the 4s channel with respectto the 4p channel increases with increasing collision energy. This can be qualitatively understood with the Landau-Zener model, because the position of the

Reproduced with permission of the copyright owner. Further reproduction prohibited without permission.

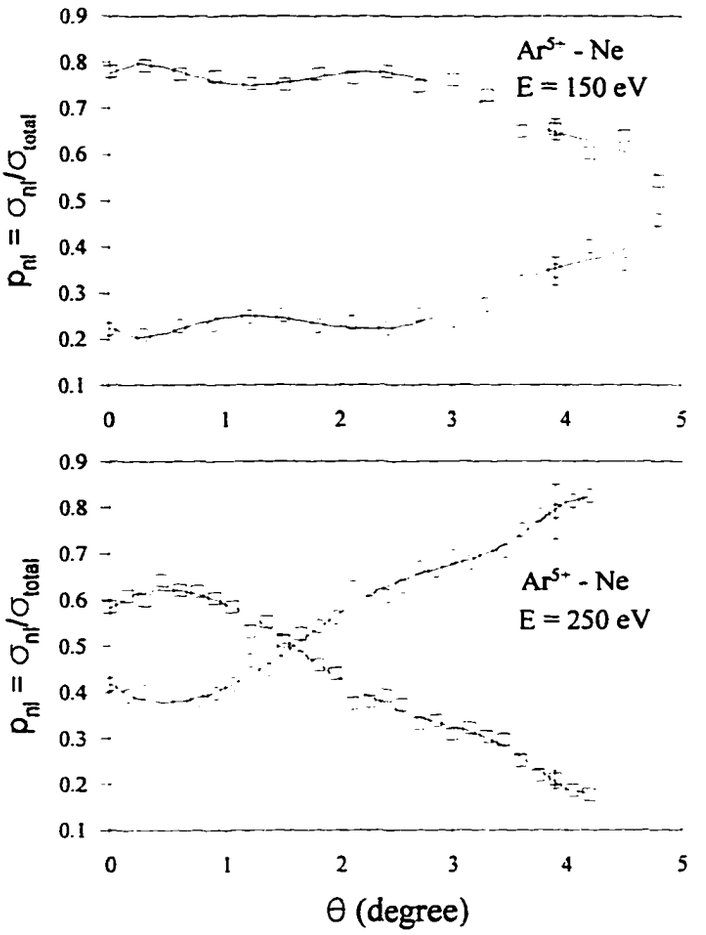

Figure 21. Probability of Single-Electron Capture by Ar^{5+} Ions From Ne as a Function of Projectile Laboratory Scattering Angle for Collision Energies 150 and 250 eV. □, 4p; ○, 4s. Smooth Lines are Drawn to Guide the Eye.

reaction window depends mainly on the collision energy of the projectile, i.e., the transition probability at the related internuclear distances increases with increasing collision energy. Figure 23 shows the dependence of the cross section ratio $\sigma(4s)/\sigma(4p)$ on the collision energy (E_{lab}), which is determined from the area under the 4s and 4p channels by fitting Gaussian peak shapes to the measured spectra presented in Figure 22.

Reproduced with permission of the copyright owner. Further reproduction prohibited without permission.

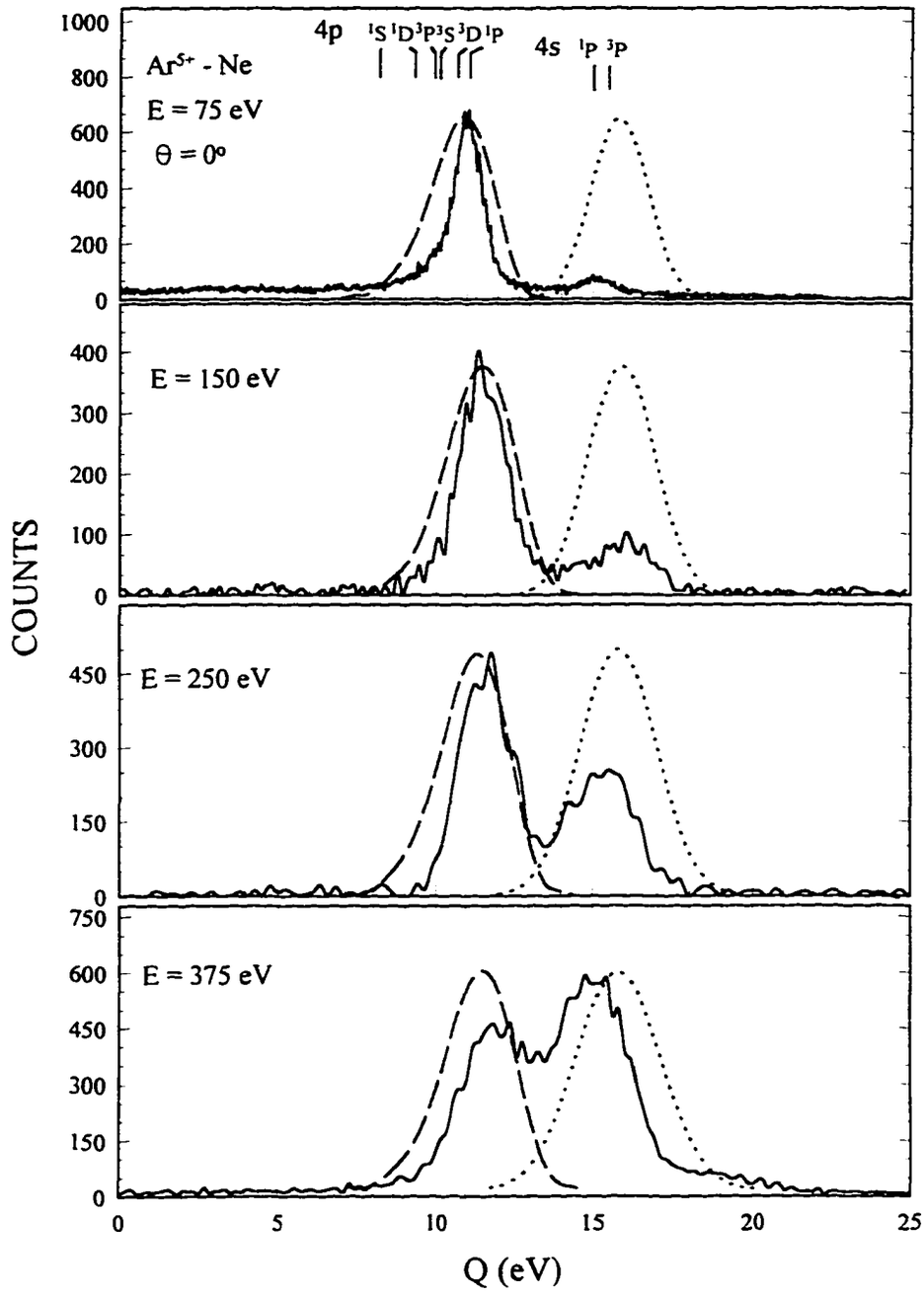

Figure 22. Translational Energy-Gain Spectra by Ar^{5+} Ions from Ne at Different Collision Energies. Also Shown are Reaction Windows Calculated on the Basis of a Single-Crossing LZ Model (Dashed Curve) and the ECOB Model (Dotted Curve).

Reproduced with permission of the copyright owner. Further reproduction prohibited without permission.

The results are compared with the multichannel Landau-Zener (MCLZ) model (Olson et al., 1976), based on the Taulbjerg expression for the coupling matrix H_{12} (Taulbjerg, 1986). It can be seen from the results displayed in Figure 23 that the ratio is an increasing function of the collision energy. The values are smaller than the MCLZ predictions by a

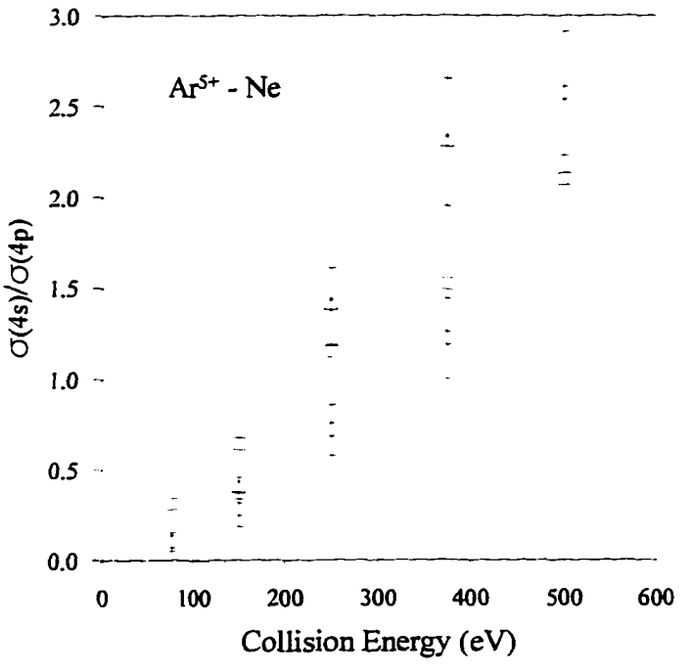

Figure 23. Collision Energy Dependence for the Ratio of Single-Electron Capture Cross Sections σ(4s)/σ(4p) in the Ar^{5+} - Ne Collision System. ○, Our Results From 0° Scattering Angle Spectra; Δ, Our Results by Integrating Differential Cross Section; □, MCLZ Predictions.

factor of 1.2 - 3, however, except at the collision energy E = 500 eV, where experiment has a larger value. This is probably due to the small angular acceptance used in the present measurements, which will underestimate the true contributions from reaction channels with large energy-gain values. However, integration of state-selective differential cross

Reproduced with permission of the copyright owner. Further reproduction prohibited without permission.

sections for capture into 4s and 4p states over an angular range 0 - 5° gives 4s/4p cross section ratios of 0.4, 1.4 and 2.3, at impact energies of 150, 250, and 375 eV, respectively.

Figure 22 also shows our calculated reaction windows for the Ar^{5+} - Ne collisions at different impact energies. For impact energies of 75, 150, and 250 eV, the reaction window based on a single-crossing LZ model provides the best description of the 4p capture channel, whereas the reaction window based on the ECOB model accommodates the 4s channel and underestimates the contribution of the 4p channel.

Ar^{6+} - Ne Collisions

Figure 24 shows the translational energy-gain spectra for single-electron capture by 300 eV Ar^{6+} ions from Ne at different projectile laboratory scattering angles. At 0° scattering angle, the dominant peak correlates with capture into the ground state of the incident Ar^{6+} ion from the 4d excited state of Ar^{5+}. There is also a significant contribution involving capture into the 4p state. As the scattering angle is increased, contributions from capture into the 4p state increase and become the dominant process at $\theta = 2.3°$. This indicates that the angular distributions for capture into 4d is more strongly peaked in the forward direction than for processes associated with capture into the 4p state. Figure 25 shows the probabilities for single-electron capture into the 4d and 4p states as a function of the projectile laboratory scattering angle for 180 and 300 eV Ar^{6+} - Ne collisions. In Figure 25, it is again demonstrated that with increasing scattering angles, contributions from avoided crossings at smaller internuclear separations (large Q-value) become

Reproduced with permission of the copyright owner. Further reproduction prohibited without permission.

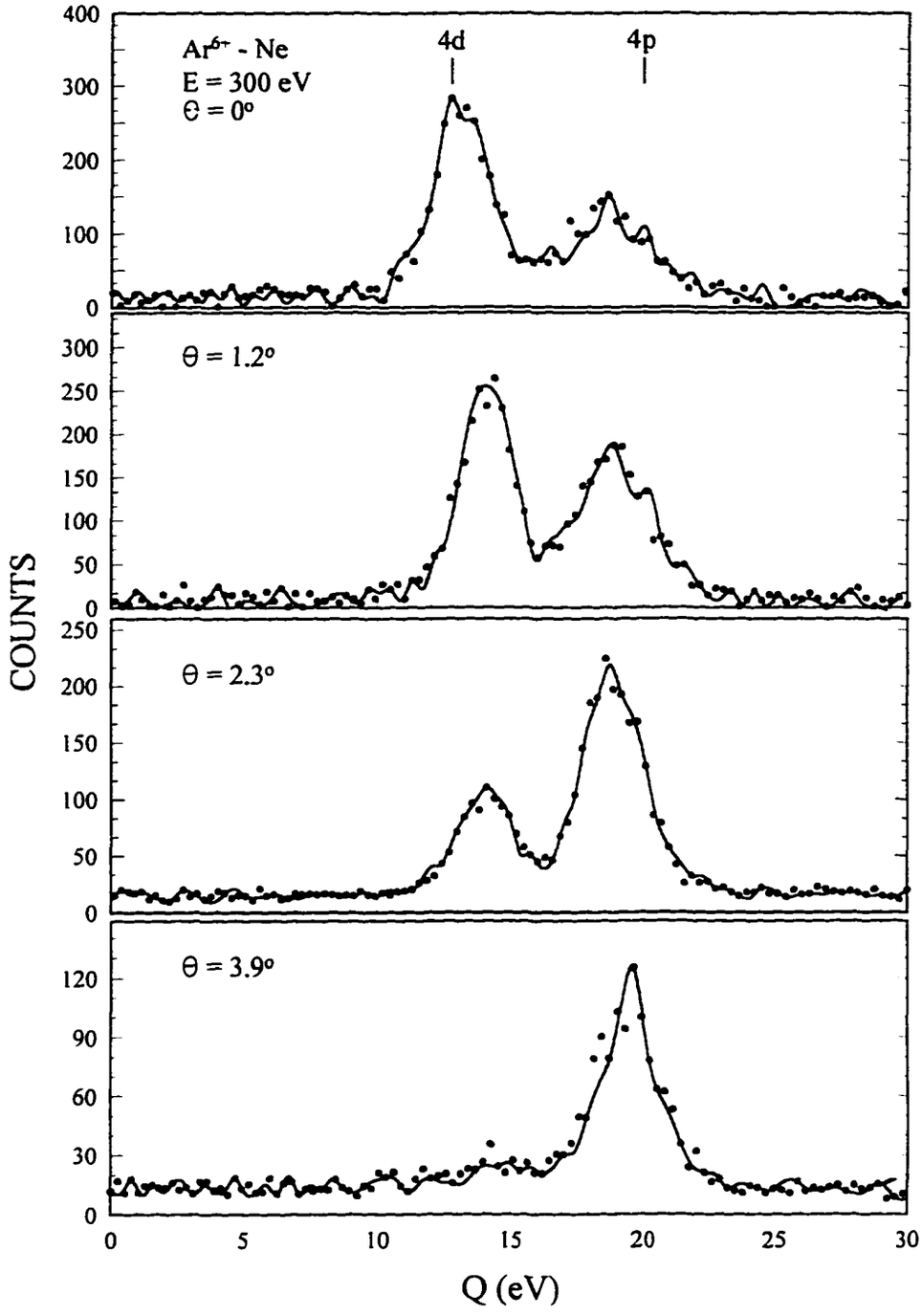

Figure 24. Translational Energy-Gain Spectra for Single-Electron Capture by 300 eV Ar^{6+} Ions From Ne at Different Projectile Laboratory Scattering Angles.

Reproduced with permission of the copyright owner. Further reproduction prohibited without permission.

gradually more important, as one would expect.

Figure 26 shows translational energy-gain spectra for single-electron capture by Ar^{6+} ions from Ne at 0° scattering angle, obtained for several collision energies. Also shown are reaction windows calculated on the basis of a single-crossing LZ model and the ECOB model. In 75 eV Ar^{6+} - Ne collisions, one peak is clearly seen; this peak correlates with capture into the ground state of the incident Ar^{6+} ions from the 4d excited state of Ar^{5+}. However, the 4p state of Ar^{5+} is found to be open at a collision energy of

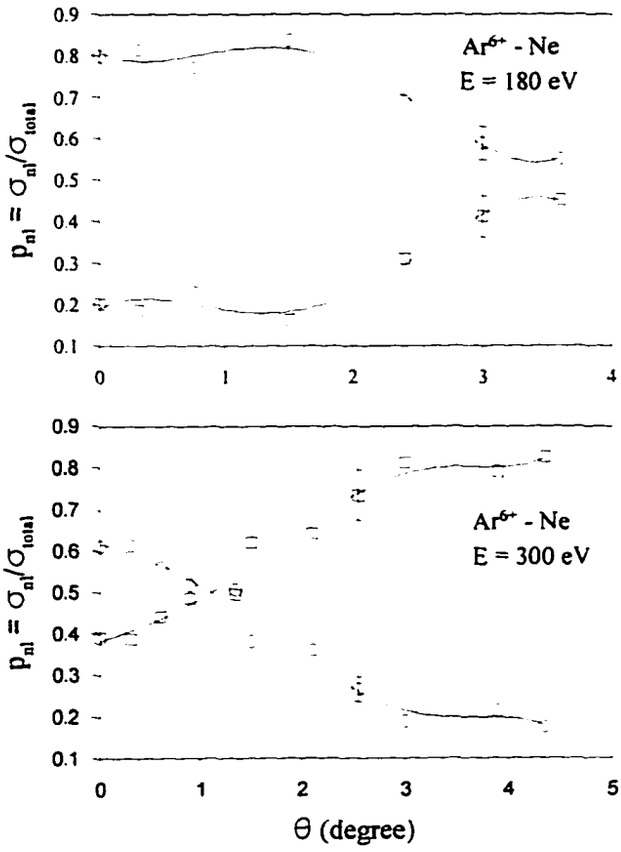

Figure 25. Probability of Single-Electron Capture by Ar^{6+} Ions From Ne as a Function of Projectile Laboratory Scattering Angle for Collision Energies of 180 and 300 eV. ○, 4d; □, 4p. Smooth Lines are Drawn to Guide the Eye.

Reproduced with permission of the copyright owner. Further reproduction prohibited without permission.

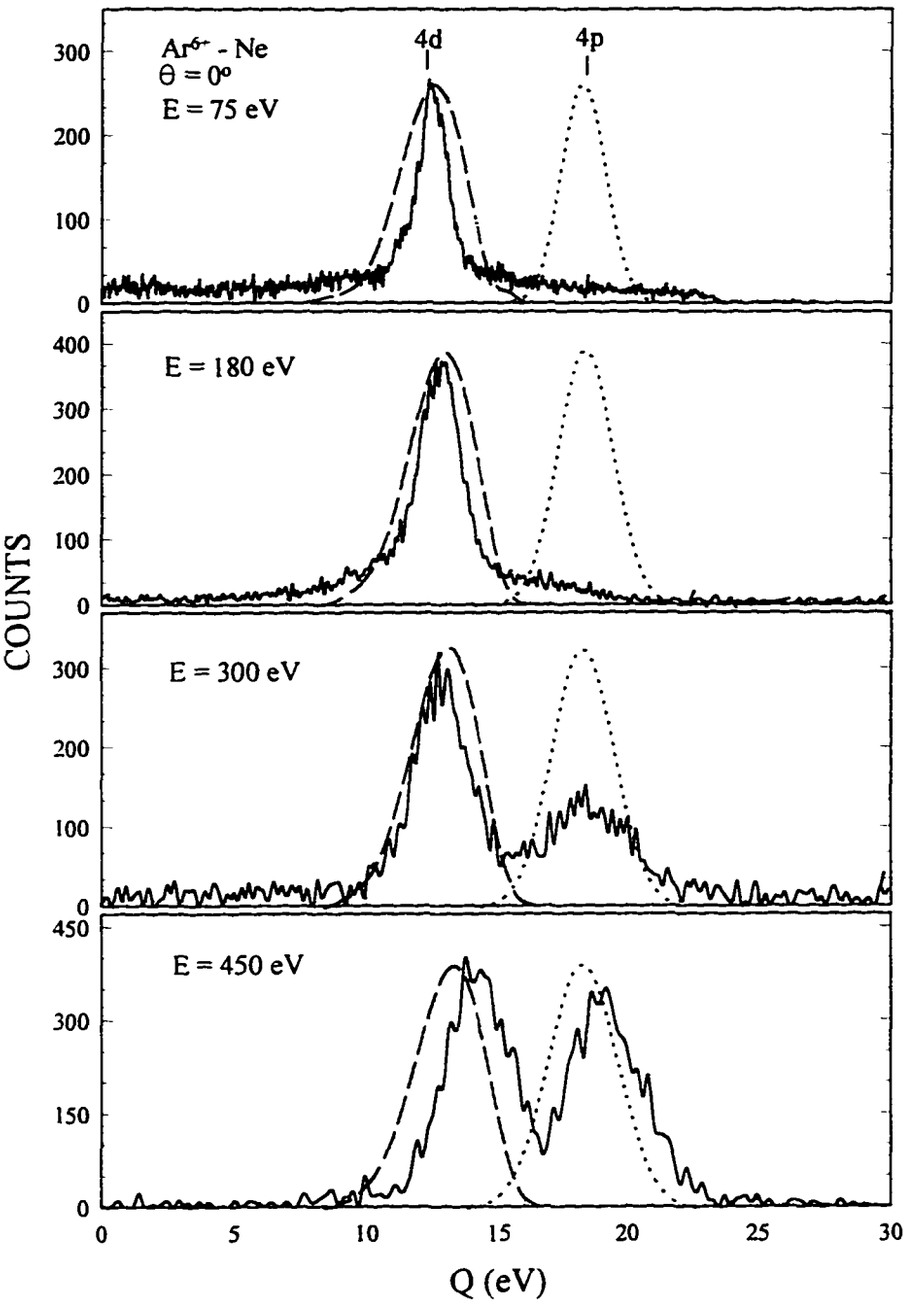

Figure 26. Translational Energy-Gain Spectra for Single-Electron Capture by Ar^{6+} Ions From Ne at Different Collision Energies. Also Shown are Reaction Windows Calculated on the Basis of a Single-Crossing LZ Model (Dashed Curve) and the ECOB Model (Dotted Curve).

Reproduced with permission of the copyright owner. Further reproduction prohibited without permission.

$E \geq 180$ eV, in agreement with the measurements of Nielsen et al. (1984). The reaction windows based on a single-crossing LZ model provide the best description of the 4d channel, while the reaction windows based on the ECOB model are positioned near the 4p channel.

The state-selective cross sections for capture into the 4d and 4p states of Ar^{5+} were integrated from the state-selective differential cross sections. The results of the ratio $\sigma(4p)/\sigma(4d)$ are shown in Figure 27 together with the measurements of Nielsen et al.

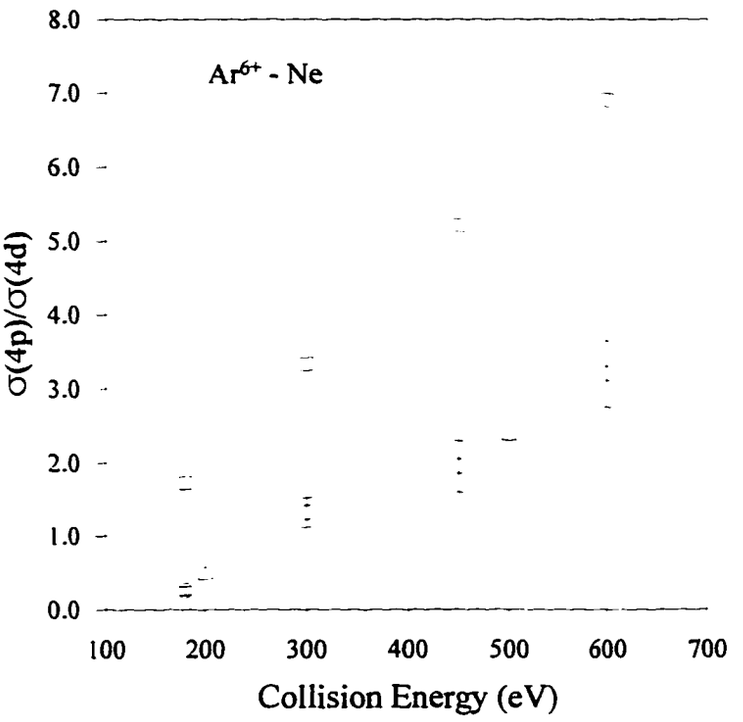

Figure 27. Collision Energy Dependence for the Ratio of Single-Electron Capture Cross Sections $\sigma(4p)/\sigma(4d)$ in the Ar^{6+} - Ne Collision System. ○, Our Results; △, Nielsen et al. (1984); □, MCLZ Predictions.

Reproduced with permission of the copyright owner. Further reproduction prohibited without permission.

(1984) at collision energies of 200 and 500 eV. For comparison, we also show, in Figure 27, the results of theoretical calculations based on the MCLZ model. It can be seen that the ratio is an increasing function of the collision energy, which is in good agreement with the results of Nielsen et al., but are a factor of 2.4 smaller than the MCLZ predictions.

Ar^{6+} - He Collisions

State-selective single-electron capture by Ar^{6+} ions from He has received extensive attention, both experimentally (Andersson, 1989; Andersson, 1991; Afrosimov, 1986; McCullough, 1987; Justiniano, 1984; Okuno, 1995) and theoretically (Opradocle, 1983; Benmeuraiem, 1987; Gargaud, 1995; Hansen, 1989) because the capture takes place mainly via few reaction channels of relatively well isolated diabatic curve crossings. Figures 28 to 30 show the translational energy-gain spectra for single-electron capture by Ar^{6+} ions from He at different projectile laboratory scattering angles and , respectively, at collision energies of 75, 150 and 300 eV.

The observed zero-angle spectra clearly indicate that single-electron capture from the ground state Ar^{6+} ($3s^2\ ^1S$) ion into the 4p state of Ar^{5+} product is the dominant reaction channel over the entire collision energy region studied, in agreement with the low-energy measurements of Andersson et al. (1989) at forward scattering angles. The unresolved structure on the lower-energy side of the dominant peak, can not be attributed to single-electron capture processes from the ground state projectile. It can however be attributed either to the presence of the metastable state Ar^{6+} ($3s\ 3p\ ^3P$) in the primary ion beam or, possibly, to transfer excitation into Ar^{5+} ($3s\ 3p(^{1,3}P)\ 3d$) configurations.

Reproduced with permission of the copyright owner. Further reproduction prohibited without permission.

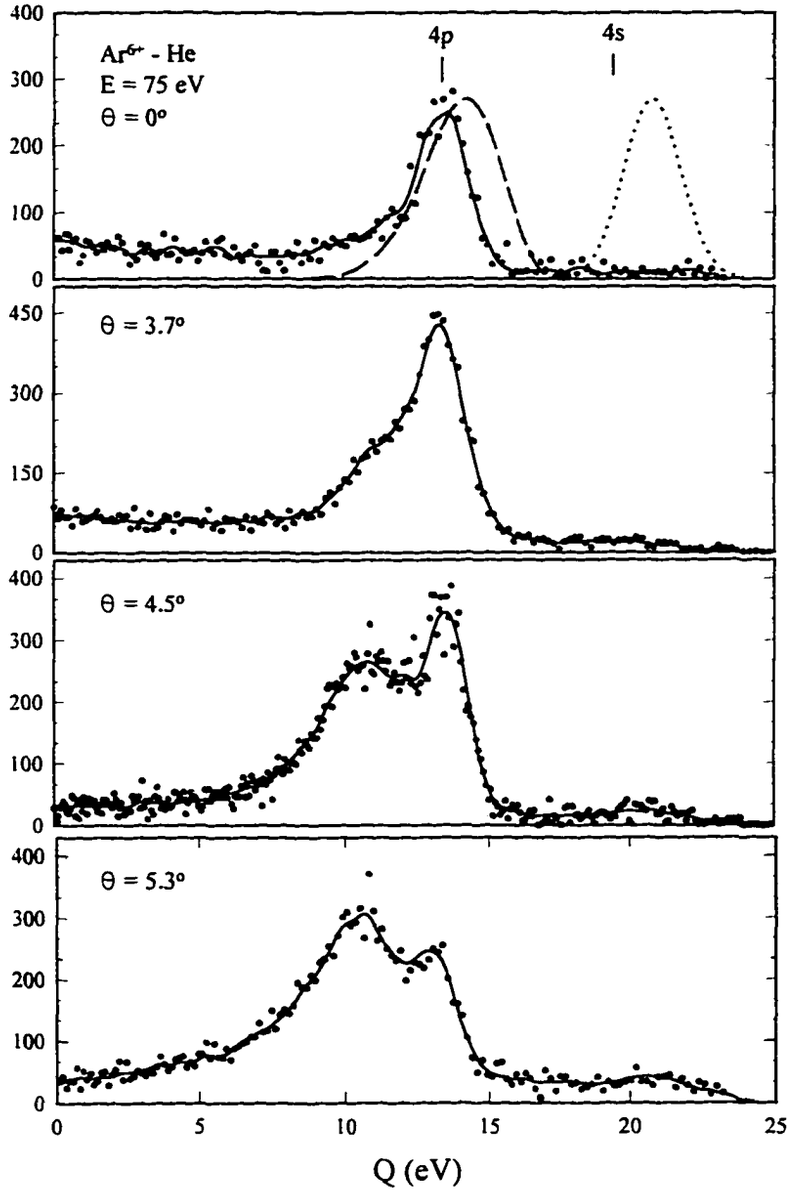

Figure 28. Translational Energy-Gain Spectra for Single-Electron Capture by 75 eV Ar^{6+} Ions From He at Different Projectile Laboratory Scattering Angles. Also Shown are Reaction Windows Calculated on the Basis of a Single-Crossing LZ Model (Dashed Curve) and the ECOB Model (Dotted Curve).

Reproduced with permission of the copyright owner. Further reproduction prohibited without permission.

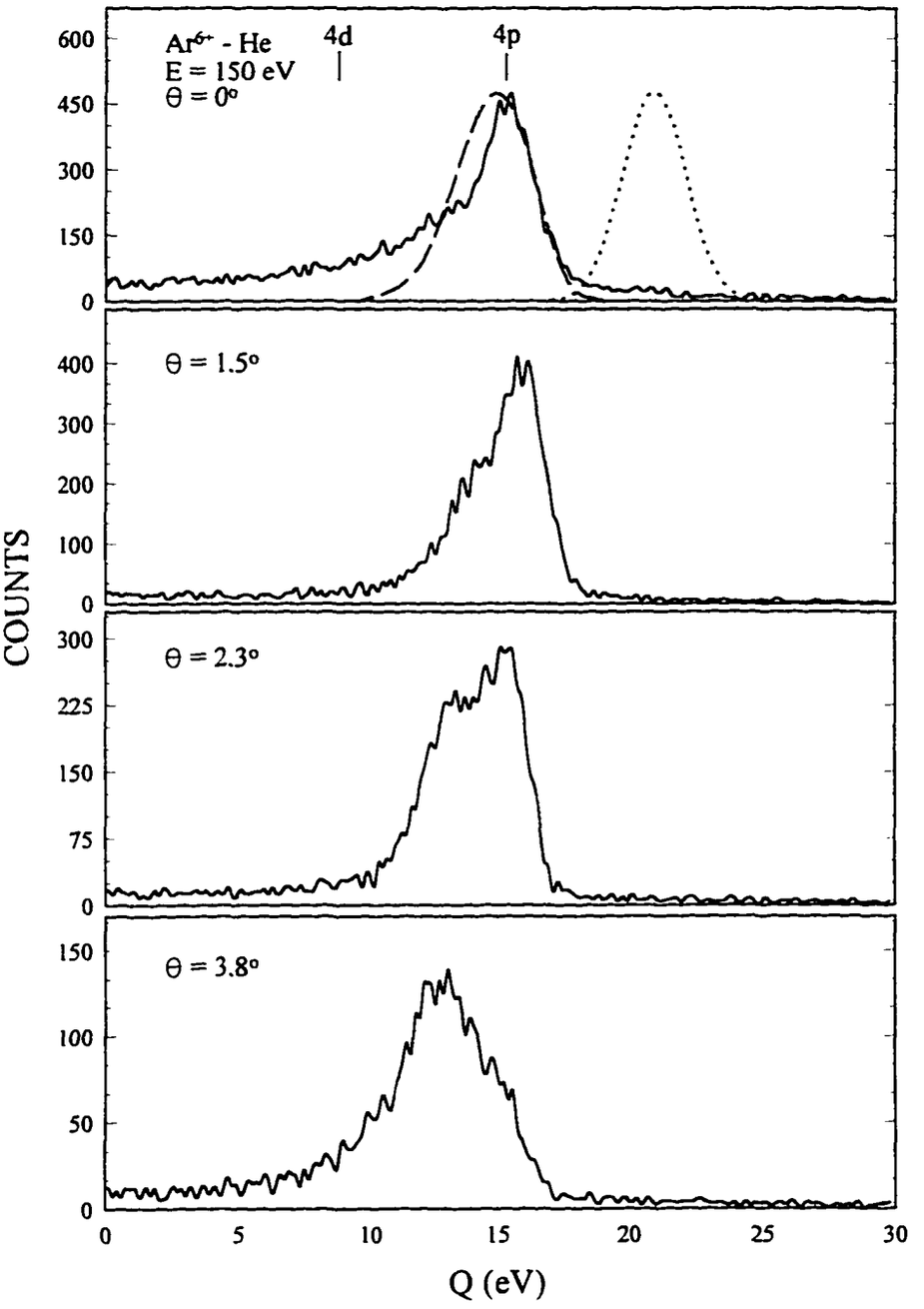

Figure 29. Translational Energy-Gain Spectra for Single-Electron Capture by 150 eV Ar^{6+} Ions From He at Different Projectile Scattering Angles. Also Shown are Reaction Windows Calculated on the Basis of a Single-Crossing LZ Model (Dashed Curve) and the ECOB Model (Dotted Curve).

Reproduced with permission of the copyright owner. Further reproduction prohibited without permission.

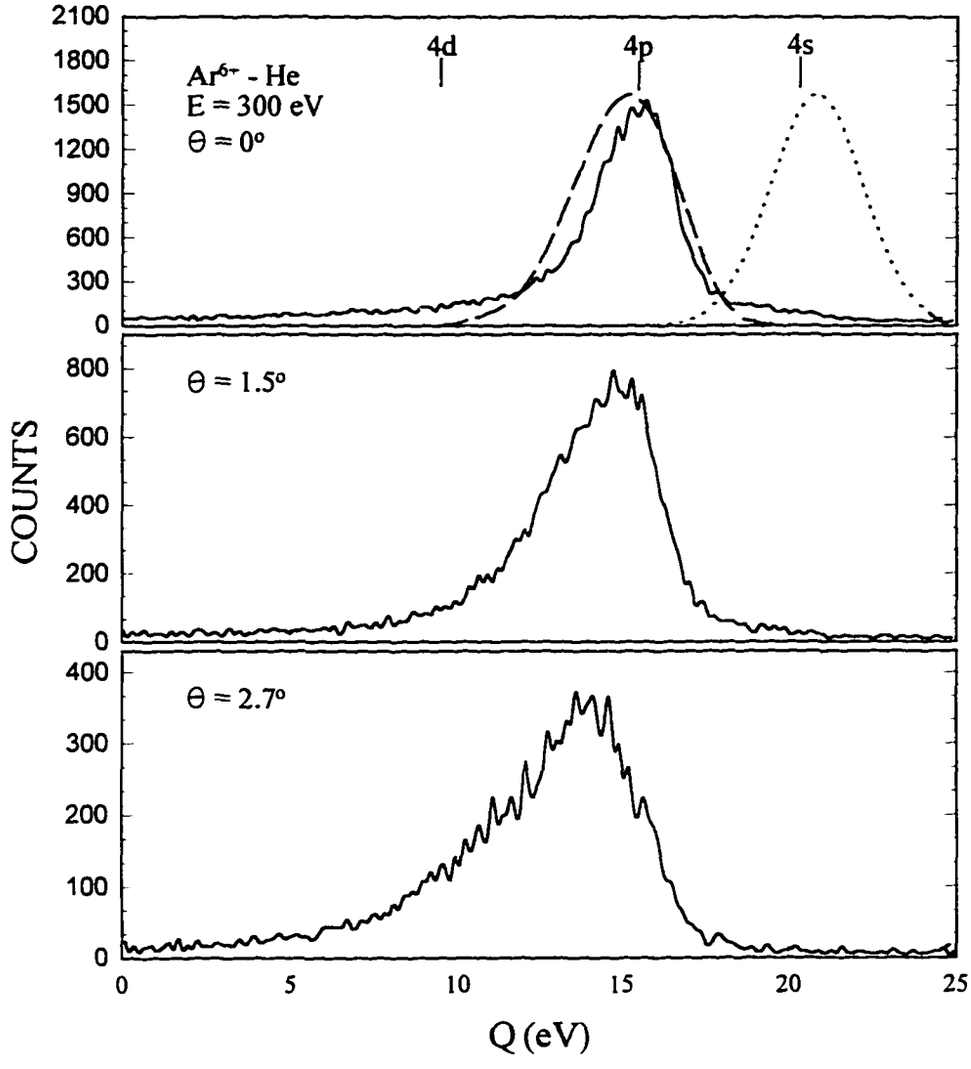

Figure 30. Translational Energy-Gain Spectra for Single-Electron Capture by 300 eV Ar^{6+} Ions From He at Different Projectile Scattering Angles. Also Shown are Reaction Windows Calculated on the Basis of a Single-Crossing LZ Model (Dashed Curve) and the ECOB Model (Dotted Curve).

Andersson et al. (1991) have improved the agreement between experimental and

Reproduced with permission of the copyright owner. Further reproduction prohibited without permission.

theoretical differential cross sections based on a simple Landau-Zener model. for Ar^{6+} - He collisions at energies below 500 eV, by including the transfer excitation channels in their calculations. Another possible explanation for this structure might be due to oscillations in the differential cross sections reflected in the translational energy-gain spectra, i.e. an effect of angular scattering (Cocke, 1989 and Andersson, 1989).

Figures 28 to 30 also show the reaction windows calculated on the basis of a single-crossing LZ model, using the Taulbjerg expression for the coupling matrix H_{12} with Taulbjerg factor $f_{nl}(4p) = 0.671$, and the ECOB model. The reaction windows based on the LZ model accommodates most of the dominant reaction channel and provides the best description of the observed spectrum, while the reaction windows based on the ECOB model favor larger energy-gain values than observed.

As the projectile laboratory scattering angle is increased, single-electron capture into the 4p state of Ar^{5+} remains dominant, but contributions from transfer excitation channels increase relative to the dominant peak and dominates at the reduced angle $\tau \geq$ 400 eV.deg, where τ is the product of the collision energy and the projectile laboratory scattering angle. This indicates that the cross sections for capture into the 4p state peaks at forward direction, while the differential cross section for transfer excitation is not maximum at 0° but instead peaks at a greater angle.

Differential Cross Sections

The experimental total differential cross sections ($d\sigma/d\Omega$) for single-electron capture by Ar^{q+} ions from He and Ne for q = 4 - 6, are shown in Figures 31 to 33. The

Reproduced with permission of the copyright owner. Further reproduction prohibited without permission.

differential cross sections were determined by the translational energy-gain technique. The area under the peaks in the energy-gain spectra at different projectile laboratory scattering angles were calculated by using a curve fitting program. The general features of the distributions are qualitatively explained in terms of classical deflection functions for the heavy particle motion.

For 200 eV Ar^{4+} - Ne collisions (see Figure 31), the distribution is peaked in the forward direction inside the critical angle $\theta_c = 1.52°$, which corresponds to the 3d ^4P capture channel at an impact parameter equal to the crossing radius, with a secondary peak at about 3°. As the projectile collision energy increases, the width of the angular distribution decreases, with distributions peaked forward more strongly inside θ_c. The forward peaks clearly represent contributions from capture into the final channel on the way-out of the collision, i.e. the lower branch of the deflection function, while the structure occurring at larger angles are almost entirely due to contributions from capture that takes place on the way into the collision, i.e. the upper branch of the deflection function.

For 150 eV Ar^{5+} - Ne collisions, the spectrum contains a forward peak inside θ_c = 2.2° for capture into the 4p state of the Ar^{4+} ion, with a secondary peak located near 2.5° (see Figure 32). The forward peak clearly represents contributions from capture on the way-out branch of the deflection function with the valley located near θ = 1.5°, which is a rainbow effect caused by 4s promotion of the entrance channel. Again, as the collision energy increases, the distributions peaks at a forward direction just inside the critical angle with some structure located outside θ_c.

Reproduced with permission of the copyright owner. Further reproduction prohibited without permission.

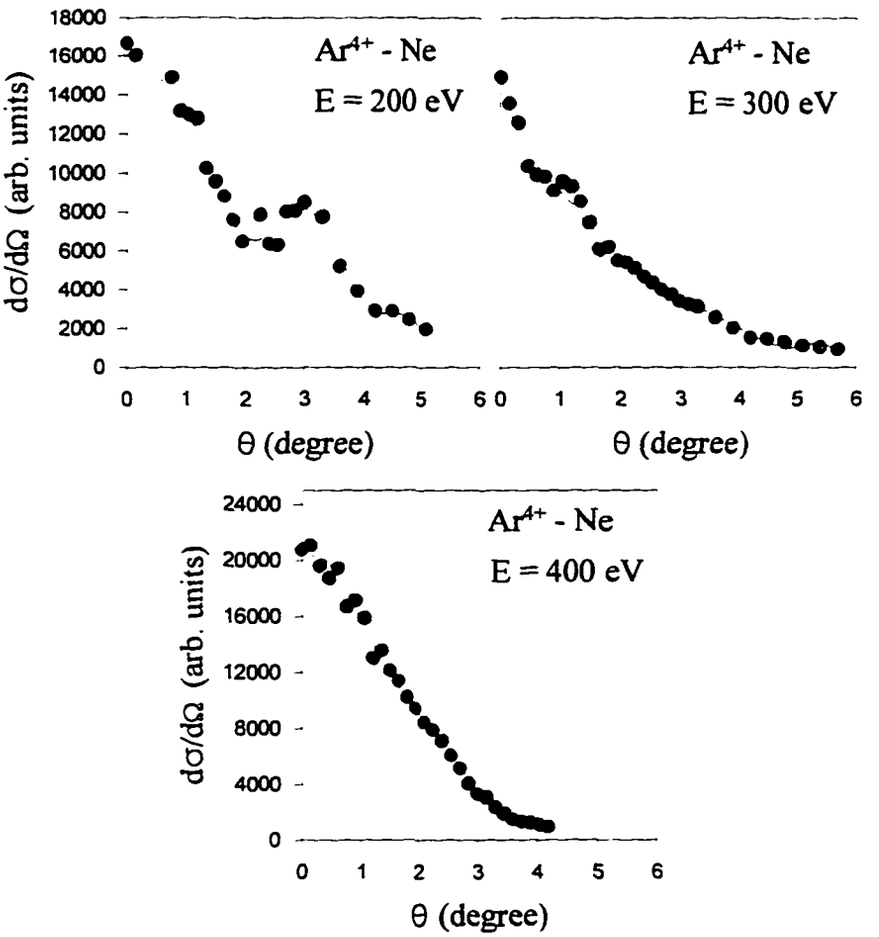

Figure 31. Experimental Differential Cross Sections ($d\sigma/d\Omega$) for Single-Electron Capture by Ar^{4+} Ions From Ne at Different Laboratory Collision Energies. Smooth Lines are Drawn to Guide the Eye.

Figure 34 displays the measured total differential cross section for single-electron capture by Ar^{6+} ions from Ne at different projectile collision energies. The measurements show that the projectile products correlate with capture into the 4d state are distributed forward inside the critical angle $\theta_c = 1.54°$, indicating that capture took place on the way out of the collision.

Reproduced with permission of the copyright owner. Further reproduction prohibited without permission.

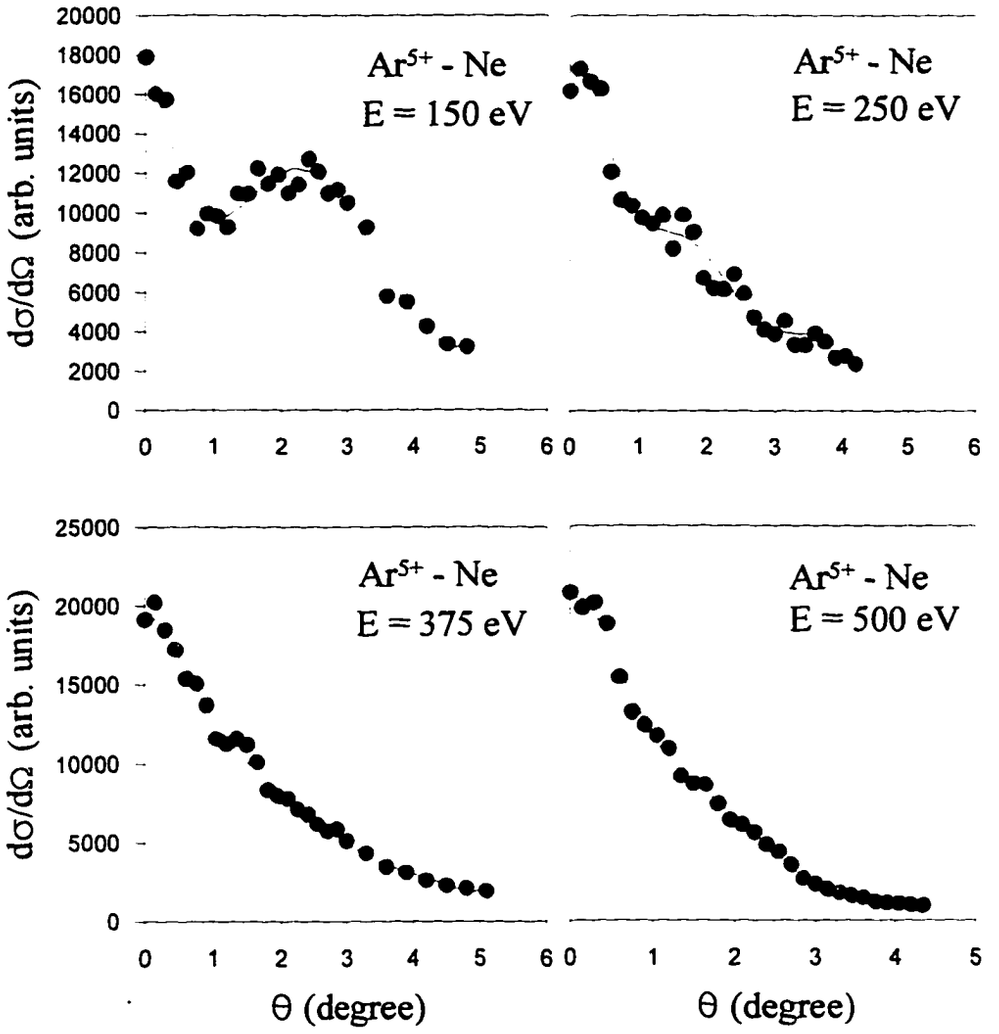

Figure 32. Experimental Differential Cross Sections ($d\sigma/d\Omega$) for Single-Electron Capture by Ar^{5+} Ions From Ne at Different Laboratory Collision Energies. Smooth Lines are Drawn to Guide the Eye.

Figure 33 shows the measured total differential cross sections for single-electron capture by Ar^{6+} ions from He at laboratory collision energies between 75 and 600 eV. At 600 eV, the distribution contains a main peak lying just inside the critical angle θ_c of 0.7° for capture into the 4p state of the Ar^{5+} ion, with a structure at about 2°. As the projectile

Reproduced with permission of the copyright owner. Further reproduction prohibited without permission.

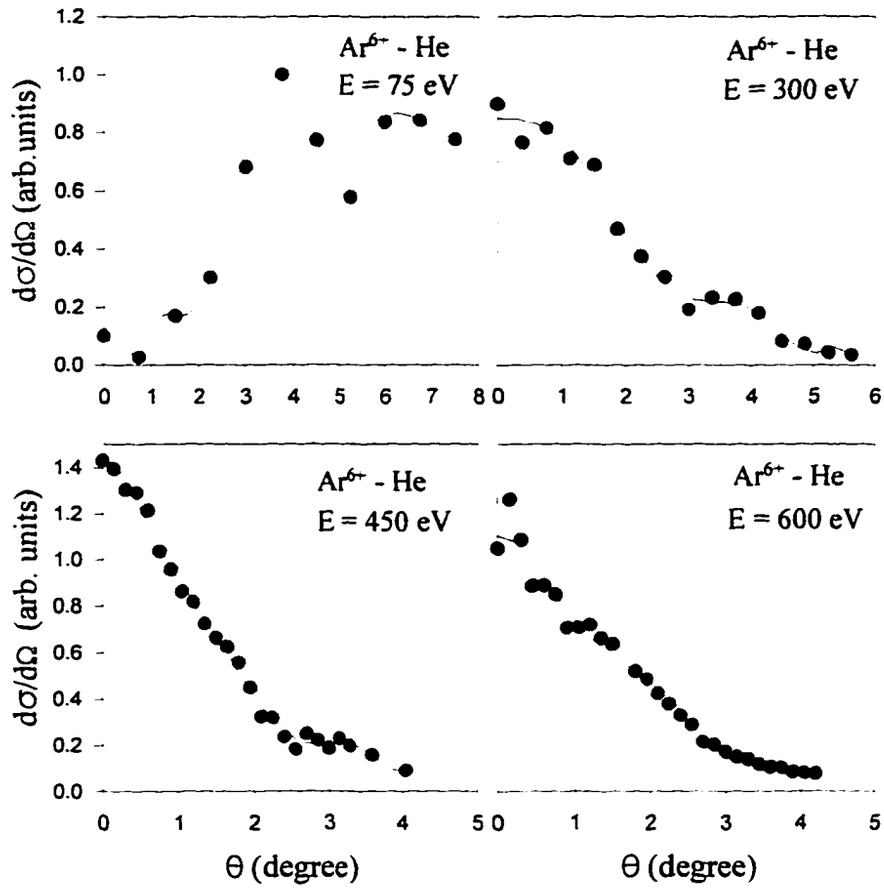

Figure 33. Experimental Differential Cross Sections ($d\sigma/d\Omega$) for Single-Electron Capture by Ar^{6+} Ions From He at Different Laboratory Collision Energies. Smooth Lines are Drawn to Guide the Eye.

collision energy decreases the contributions inside θ_c increase in magnitude. At 75 eV, the data show that the distribution is peaked at 4° with a secondary peak at about 6° just outside θ_c. The primary peak clearly represents contribution from capture into the 4p channel on the way into the collision, while the second peak consists almost entirely of contributions from capture on the way out of the collision.

Using a multistate collision model based on classical trajectories for nuclear

Reproduced with permission of the copyright owner. Further reproduction prohibited without permission.

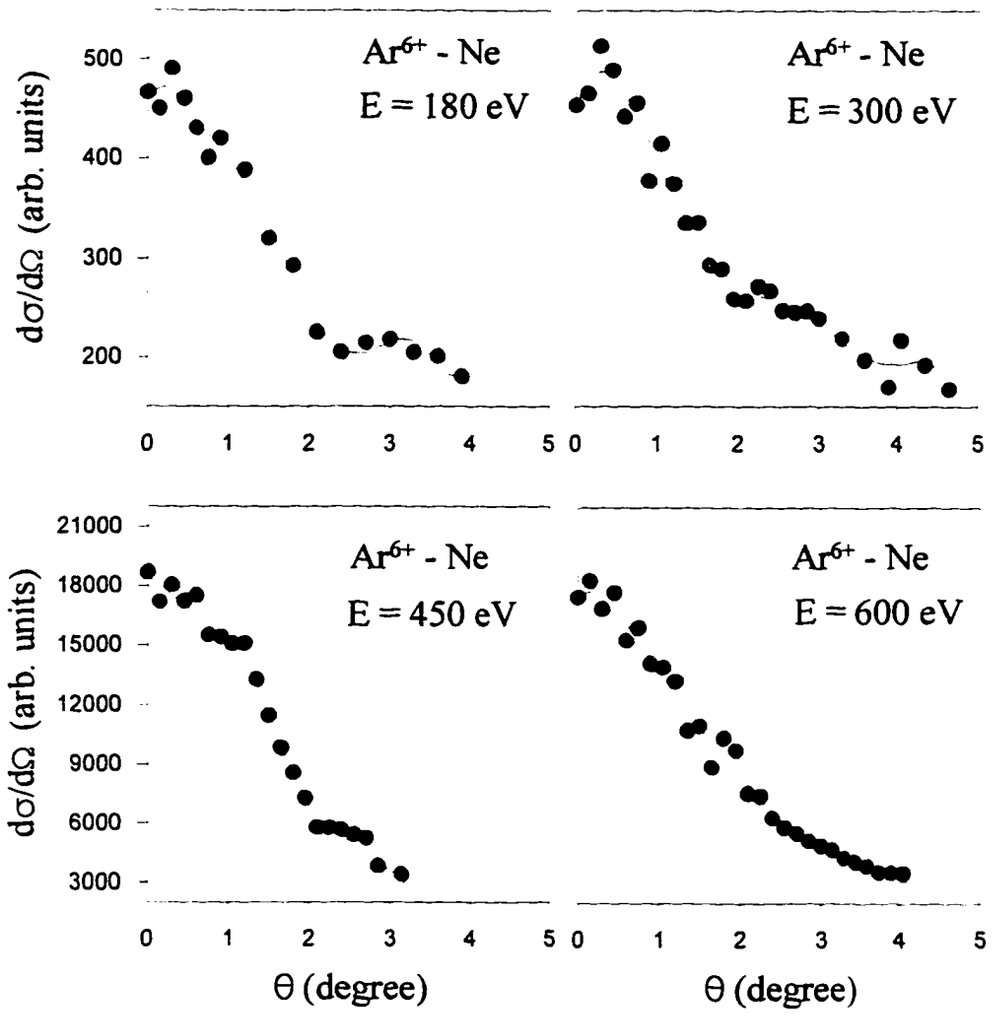

Figure 34. Experimental Differential Cross Sections ($d\sigma/d\Omega$) for Single-Electron Capture by Ar^{6+} Ions From Ne at Different Laboratory Collision Energies. Smooth Lines are Drawn to Guide the Eye.

motion and multichannel Landau-Zener transition probabilities which have been described in detail by Andersson et al., (1987), we have performed calculations for selected collision systems to interpret the measured differential cross sections. The experimental cross sections and the theoretical calculations folded with the experimental resolution are shown

Reproduced with permission of the copyright owner. Further reproduction prohibited without permission.

in Figure 35. The value of the largest calculated cross section has been normalized to the height of the peak observed in the spectrum.

For the 200 eV Ar^{4+} - Ne collisions, the calculation is performed assuming the 3d ^4P and $3p^4\ ^2S$ states of the Ar^{3+} ion to be open channels, with the $3p^4\ ^2S$ channel taken to be the promotion channel. The calculation reproduces the forward peak, but it is narrower than the experimental distribution and underestimates the contribution from capture on the way out of the collision (note the secondary structure located near θ =3°). In order to obtain better agreement with the experimental distribution, one must take into account the contributions due to capture into the core-excited $3p^2(^1D)3d$ states, which was ignored in the calculation.

For the 150 eV Ar^{5+} - Ne collisions, the calculation, which is performed assuming that the 4p, 4s, and 3d channels contribute to single-electron capture with the 3d channel as the promotor, correctly predict the location of the secondary peak. However, the calculation underestimates the contribution from capture that takes place on the way out of the collision.

For the 600 eV Ar^{6+} - Ne collisions, the calculation is constructed assuming the 4s channel is the promoting channel with contributions from capture into the 4d, 4p, and 4s states. The data and calculation appear to be in good agreement. For the 75 eV Ar^{6+} - He collisions, the calculation, which assumed that the 4d, 4p and 4s capture channels were open and 4p was the promoting channel, underestimates the contribution due to capture on the way into the collision. However, the calculation correctly predicts the position of the main peak, which corresponds to an electron being captured on the way

Reproduced with permission of the copyright owner. Further reproduction prohibited without permission.

out of the collision. Andersson et al. (1991) have improved the agreement between the calculated and the experimental differential cross sections for Ar^{6+} - He collisions at energies below 400 eV, by including the $3s3p(^{1,3}P)3d$ states in their calculations using a

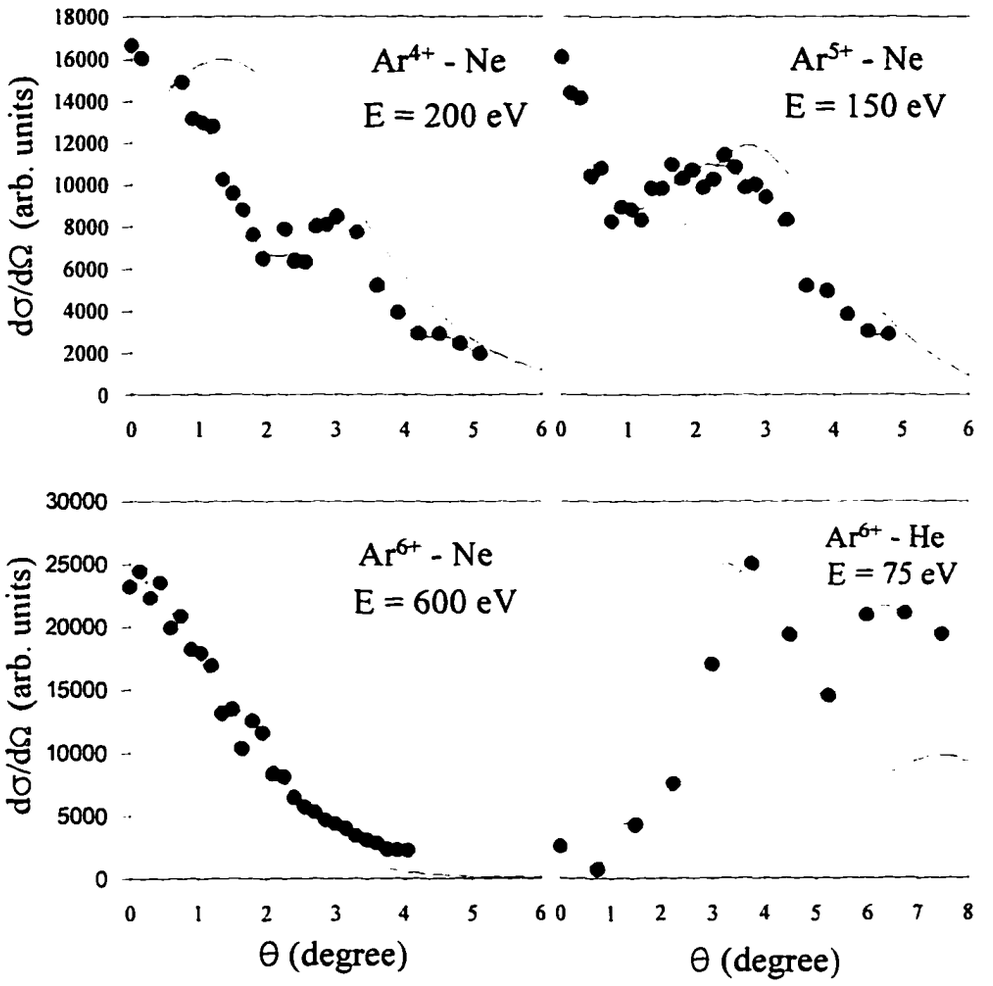

Figure 35. Experimental and Calculated Differential Cross Sections ($d\sigma/d\Omega$) for Single-Electron Capture From He and Ne by Ar^{q+} Ions (q = 4 - 6). ●, Present Results; the Dashed Curves are the Theoretical Calculations Folded With Experimental Resolutions. Smooth Lines are Drawn to Guide the Eye.

Reproduced with permission of the copyright owner. Further reproduction prohibited without permission.

modified version of the MCLZ model.

Total Cross Sections

We have measured total cross sections for single-electron capture by Ar^{q+} ions (q = 4 - 8) from He and Ne at laboratory collision energies between 15 and 100 qeV. Our results are displayed in Figures 36 and 37 together with other available measurements and compared to those theoretical values obtained by the Landau-Zener model (Landau, 1932; Zener, 1932), absorbing sphere model (Olson et al., 1976), classical over barrirer model (COB) (Ryfuku, 1980), and Muller-Salzborn scaling law (Muller et al., 1977). Also in Table 4 our experimental cross sections results are numerically displayed.

Except for the single-electron capture by Ar^{4+} ions from He and Ne, the total cross sections show no significant dependence on the collision energy, a behavior which is well documented for such collisions at low energies. This is attributed to the availability of many capture channels, which are situated nearly at the center of the reaction window. For Ar^{4+} ions, the total cross section slowly increases with increasing collision energies. This can be also understood from the reaction window, which gets broader with increasing energy and therefore the capture channels with large Q values get an increasing probability.

The present measurements are at least a factor of 3 smaller than the absorbing sphere model predictions. However, except for Ar^{7+} - Ne and Ar^{8+} - Ne collisions, cross sections are in good agreement with the Muller-Salzborn scaling law.

For Ar^{6+} - He collisions, our results are in reasonably good agreement with the

Reproduced with permission of the copyright owner. Further reproduction prohibited without permission.

experimental results of Andersson et al. (1989) and Andersson (1993) at low energies (≤300 eV) and show similar behavior (cross sections slowly increase with increasing impact energies). However, our data are considerably lower than the data of Okuno et al. (1995), which decrease with increasing energy. For impact energies E ≥ 450 eV, our data are in good agreement with the data of Justiniano et al. (1984) and Mann (1986), but are lower than those of Andersson (1993) and Okuno et al. (1995) by a factor of 1.6. In the low energy region, the present results are found to be 7% smaller than those theoretical results of Gardaud et al. (1995), Andersson (1993), and multichannel Landau-Zener calculations (Olson et al. 1976), which are based on the Taulbjerg expression for the coupling matrix H_{12} (Taulbjerg, 1986). However, they are in good accord with our cross section at 900 eV. For Ar^{8+} - He collisions, our experimental results for collision energies E ≥ 400 eV are in good agreement with the data of Okuno et al. (1995) and Nielsen et al. (1985).

For Ar^{q+} - Ne collisions, our data are lower than the results of Suzuki et al. (1997) which exhibited similar behavior for the Ar^{6+} - He collision system (the cross section increase with decreasing collision energy), except for Ar^{4+} - Ne collisions, which slowly decrease with decreasing energy, a feature similar to our results (see Figure 37). However, our experimental results for single-electron capture by Ar^{6+} and Ar^{8+} ions from Ne are in good agreement with the results of Nielsen et al. (1985).

The dependence of the single-electron capture cross section on the initial projectile charge state of 100 qeV Ar^{q+} ions in collisions with He and Ne are shown in Figures 38 and 39, respectively. The predictions of the absorbing sphere model, the Muller-Salzborn

Reproduced with permission of the copyright owner. Further reproduction prohibited without permission.

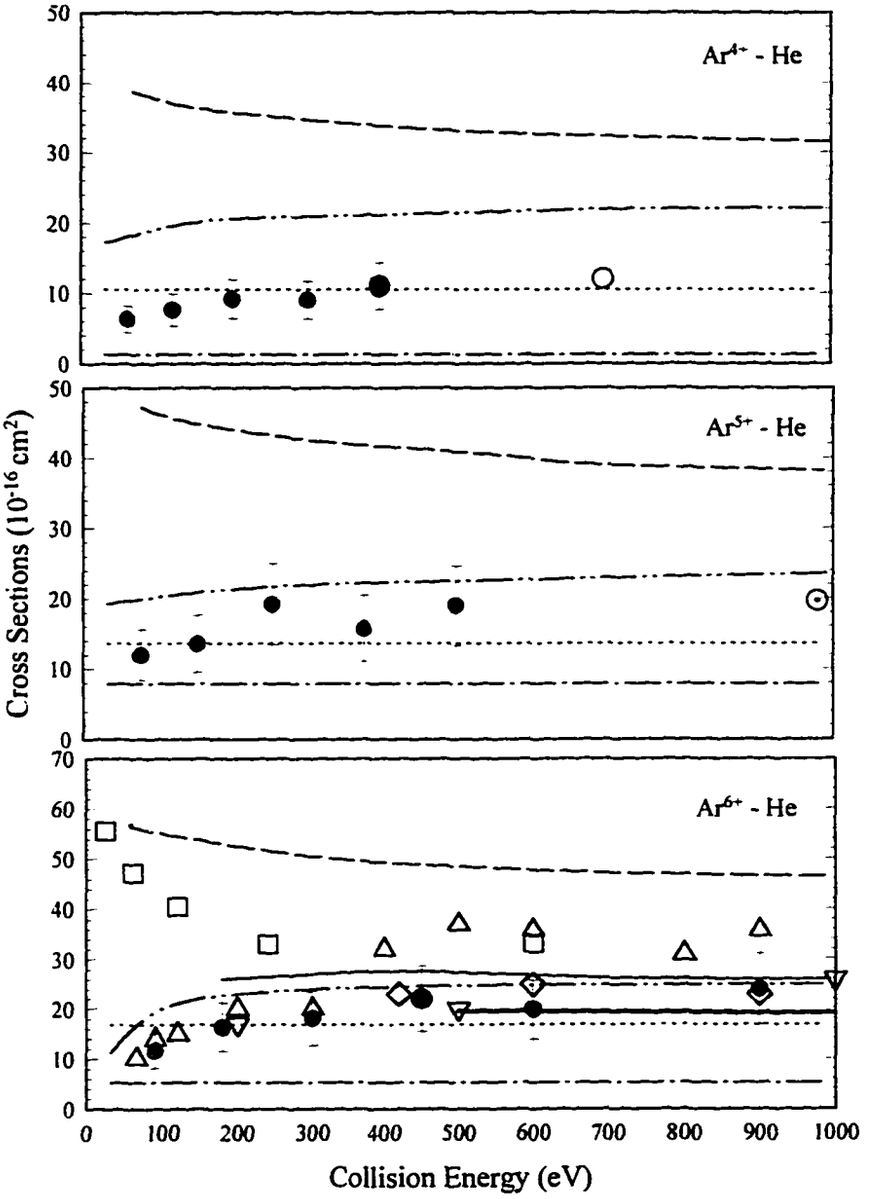

Figure 36. Total Cross Sections for Single-Electron Capture by Ar^{q+} Ions (q = 4 - 8) From He. ●, Present Work; □, Okuno et al. (1995); △, Andersson et al. (1993); ○, Justiniano et al. (1984); ▽, Andersson et al. (1989); ◇, Gosselin (1993); ⊙, Mann (1986); Solid Curve, Gardaud et al. (1995); Thick Solid Line, Hansen et al. (1989); Dashed Curve, Absorbing Sphere Model; Dot-Dash Curve, COB Model; Two Dots-Dash Curve, MCLZ Calculations; Dotted Curve, Muller-Salzborn Scaling Law.

Reproduced with permission of the copyright owner. Further reproduction prohibited without permission.

Figure 36 - Continued

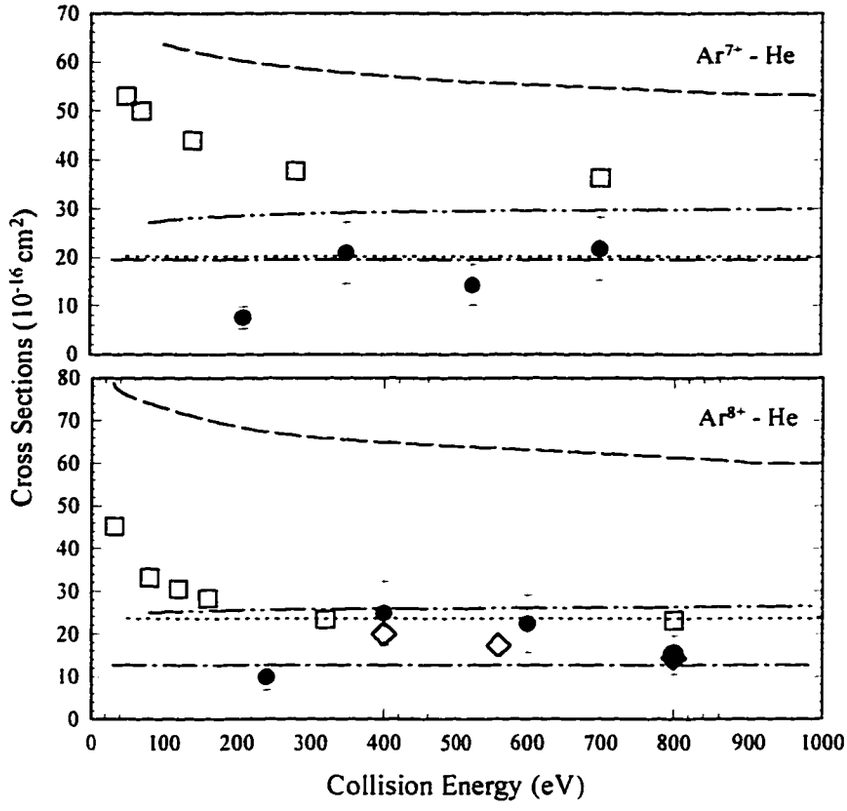

scaling law, LZ model, and the classical over-barrier model (which were discussed in Chapter 3), together with other measurements are also shown in the Figures 38 and 39 for comparison. The cross section increases with the charge state, although some oscillations are observed. Such oscillations in total cross section have also been reported by other investigators for similar collision systems (Nielsen et al., 1984; Justiniano et al., 1984; Mann, 1986). The absorbing sphere model and the Muller-Salzborn scaling law do not predict an oscillatory dependence on the charge state but a smooth increase of the cross section with the charge state. The predictions of the scaling law seems to follow the

Reproduced with permission of the copyright owner. Further reproduction prohibited without permission.

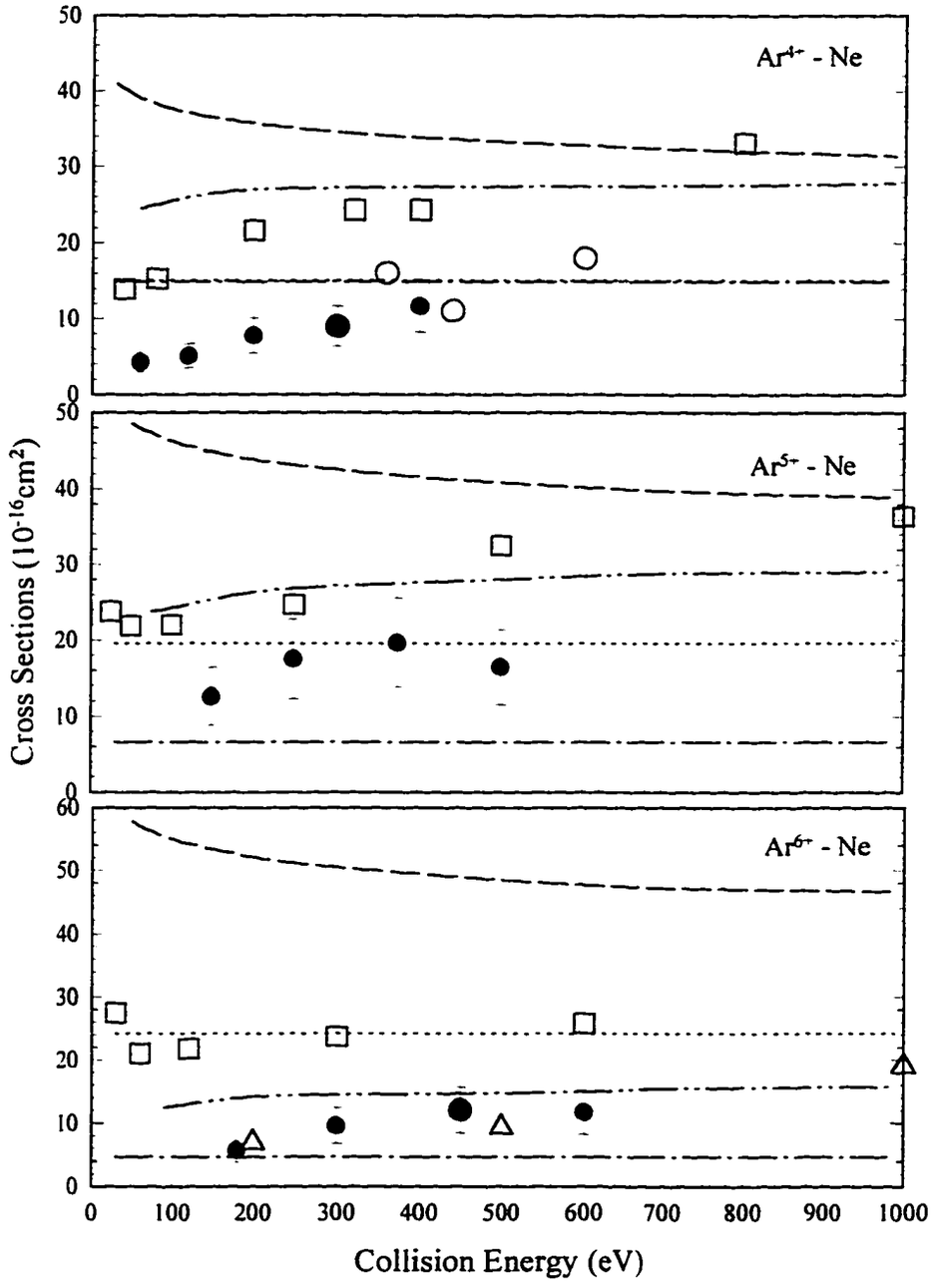

Figure 37. Total Cross Sections for Single-Electron Capture by Ar^{q+} Ions (q = 4 - 8) From Ne. ●, Present Work; □, Suzuki et al. (1997); ○, Justiniano et al. (1984); Δ, Nielsen et al. (1985); Dashed Curve, Absorbing Sphere Model; Dot-Dash Curve, COB Model; Two Dots-Dash Curve, MCLZ Calculations; Dotted Curve, Muller-Salzborn Scaling Law.

Reproduced with permission of the copyright owner. Further reproduction prohibited without permission.

Figure 37 - Continued

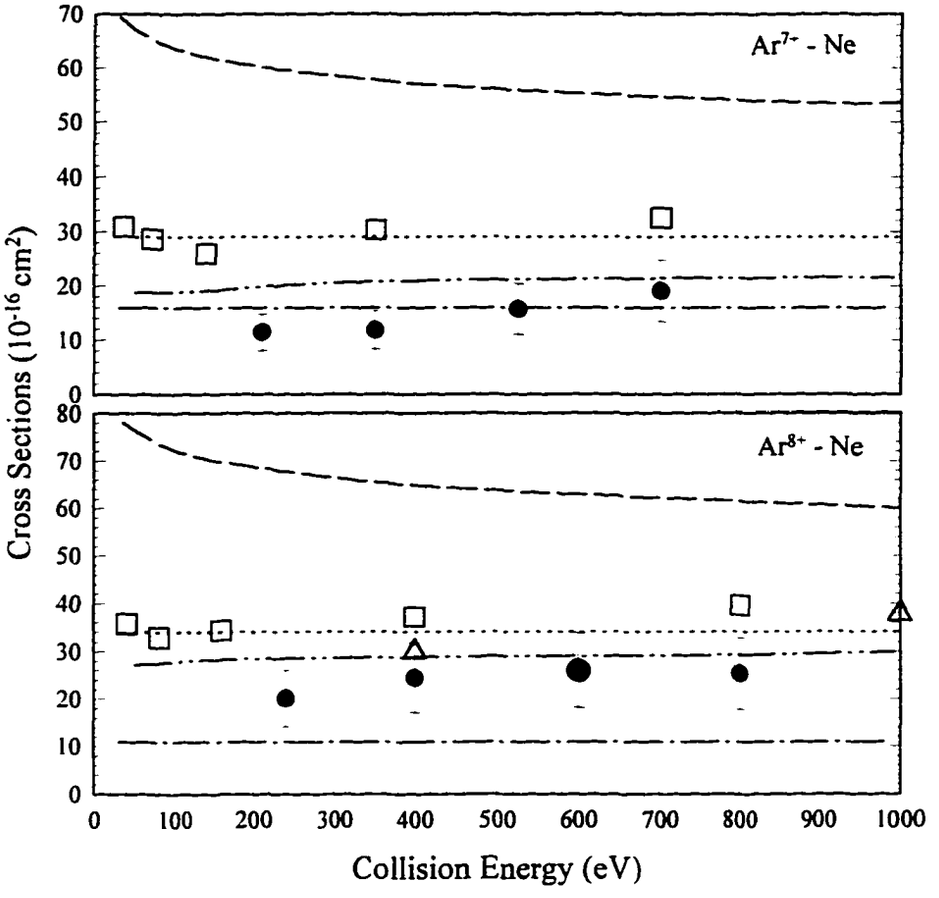

trend of the measured cross section, but significant differences are observed when the measured values are compared with the predictions of the absorbing sphere model. The overestimated results of the absorbing sphere model can be understood in terms of the lack of a high density of capture channels especially, for low charge state, since the predictions of the model are the maximum cross sections which are expected to provide reasonable agreement only for the high charge states.

Figure 38 compares our data for He targets with those of Justiniano et al. (1984),

Reproduced with permission of the copyright owner. Further reproduction prohibited without permission.

Table 4

Present Experimental Cross Sections for Single- Electron Capture by Ar^{q+} (q = 4 - 8) Ions From He and Ne. The Units of Collision Energy and Cross Sections are, respectively, qeV and $10^{-16}cm^2$

Ar^{q+} - He

E	q = 4	q = 5	q = 6	q = 7	q = 8
15	6.3	12.0	11.6	-	-
30	7.6	13.5	16.2	7.5	9.9
50	9.1	19.2	18.1	20.9	24.9
75	9.0	15.7	22.0	14.2	22.4
100	11.0	19.0	19.8	21.7	15.0

Ar^{q+} - Ne

E	q = 4	q = 5	q = 6	q = 7	q = 8
15	4.3	-	-	-	-
30	5.1	12.6	5.5	11.4	20.1
50	7.8	17.5	9.5	11.9	24.5
75	9.0	19.7	12.0	15.7	26.0
100	11.7	16.4	11.7	19.0	25.3

Mann (1986), and Okuno et al. (1995), respectively, at impact energies of 500, 198, and 100 qeV. Our data are in good agreement, within the absolute uncertainties, with the results of Justiniano et al. (1984) and Mann (1986), but are a factor of 1.5 smaller than the results of Okuno et al. (1995). Cross Sections for single-electron capture by 100 qeV Ar^{q+} ions from Ne are displayed as function of the projectile charge state in Figure 39, together with measurements of Justiniano et al. (1984), Nielsen et al. (1985), and Suzuki et al. (1997). Our results are in good agreement with the results of Justiniano et al. (1984), but lower than the results of Suzuki et al. (1997) and Nielsen et al. (1985).

Reproduced with permission of the copyright owner. Further reproduction prohibited without permission.

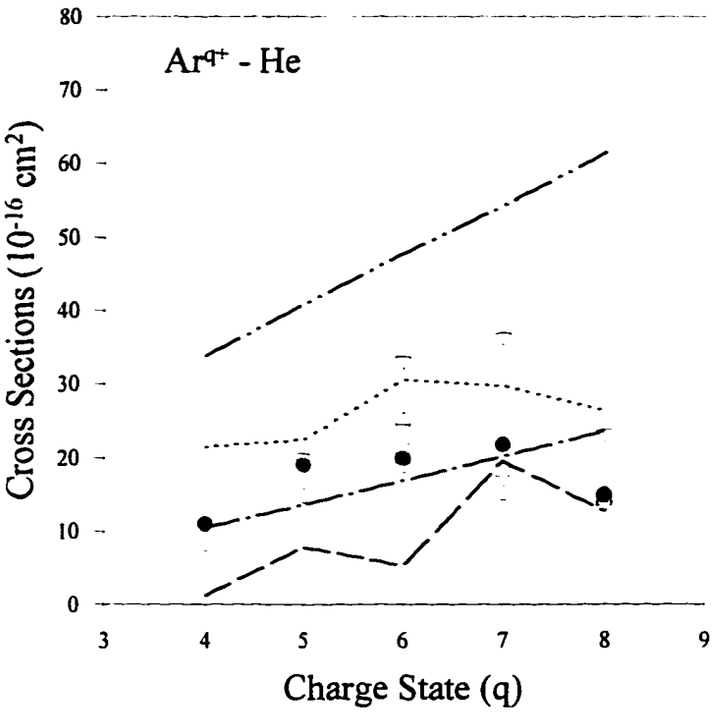

Figure 38. Total Cross Sections for Single-Electron Capture by Ar^{q+} Ions (q = 4 - 8) From He. ●, Present Work, E = 100 qeV; ○, Justiniano et al. (1984), E = 500 qeV; □, Mann (1986), E = 198 eV; ▽, Okuno et al. (1995), E = 100 qeV; △. Gosselin (1993), E = 100 qeV; Dot-Dash Curve, Muller-Salzborn Scaling Law; Dotted Curve, MCLZ Calculations; Two Dot-Dash Curve, Absorbing Sphere Model; Dashed Curve, COB Model.

Reproduced with permission of the copyright owner. Further reproduction prohibited without permission.

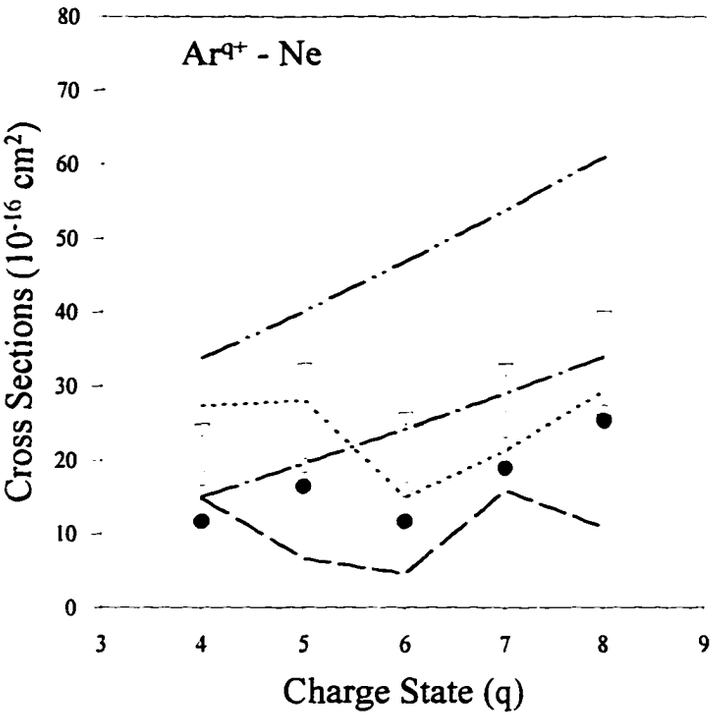

Figure 39. Total Cross Sections for Single-Electron Capture by Ar^{q+} Ions (q = 4 - 8) From Ne. ●, Present Work, E = 100 qeV; ○, Justiniano et al. (1984), E = 500 qeV; ∇, Suzuki et al. (1997), E = 100 qeV; ◊, Nielsen et al. (1985). E = 1000 eV; Dot-Dash Curve, Muller-Salzborn Scaling Law; Dotted Curve. MCLZ Calculations; Two Dot-Dash Curve, Absorbing Sphere Model; Dashed Curve, COB Model.

Reproduced with permission of the copyright owner. Further reproduction prohibited without permission.

CHAPTER VI

CONCLUSION

Doubly differential cross sections, in energy and angle, for single-electron capture by very low-energy Ar^{q+} ions ($q = 4 - 6$) from Ne and Ar^{6+} ions from He have been studied by means of translational energy-gain spectroscopy. The translational energy-gain spectra show that only a few states are populated depending on the charge state of the projectile, projectile laboratory scattering angle, and the collision energy. The translational energy-gain spectra were interpreted qualitatively in terms of the reaction windows, which are calculated using the single-crossing LZ model and the ECOB model. The reaction windows based on a single-crossing LZ model provide the best description of the position of the dominant reaction channels, while the reaction windows based on the ECOB model favor Q values larger than those of the dominant processes. The relative cross sections for capture channels were measured and found to be in reasonably good agreement with the MCLZ model predictions.

We have also studied differential cross sections for single-electron capture processes in the mentioned collision systems. The angular distribution spectra contain a main peak lying just inside a critical angle θ_c, corresponding to capture at an impact parameter equal to the crossing radius of the dominant reaction channel. The peaks are qualitatively explained by a multistate collision model and are attributed to the capture

Reproduced with permission of the copyright owner. Further reproduction prohibited without permission.

process on the way out of the collision. In order to improve agreement of calculations with the experimental results, the contributions due to transfer excitation processes should be included in the calculations, using a modified version of the MCLZ model which was not available for comparison with these measurements.

The energy dependence of cross sections for single-electron capture by Ar^{q+} ions (q = 4 - 8) from He and Ne of the present work were compared with the available data and the predictions of the theoretical models. The cross sections for single-electron capture by $Ar^{(6+,7+)}$ ions from He and Ar^{q+} ions (q=4-8) from Ne are smaller by roughly a factor of 2 than the cross sections measured by Okuno et al. (1995) and Suzuki et al. (1997), respectively. However, the present data for the collision system Ar^{8+} - He agree reasonably with the data measured by Okuno et al.(1995) and Andersen et al. (1989). In the case of Ar^{6+} - He collisions, there is good agreement between the present data and the cross sections measured by Gosselin (1989), Andersson et al. (1989), and Andersson (1993) for E $\leq$ 400 eV. For the case of Ar^{6+} ions on Ne, our results are quite consistent with the results of Nielsen et al.(1984).

The measured single-electron capture cross sections for Ar^{q+} - He and $Ar^{(4+,5+)}$ - Ne collisions agrees with the Muller-Salzborn scaling law, whereas the absorbing sphere model overestimates the cross sections by a factor of 3-4. The COB calculations lie about 40 - 60% below the experimental values for $Ar^{(4+,6+)}$ - He and $Ar^{(5+,6+,8+)}$ - Ne collision systems, but agrees with the mean values of the present data for collision systems $Ar^{(7+,8+)}$ - He and Ar^{7+} - Ne. The MCLZ model overestimates the cross sections for the Ar^{q+} - He collisions, but is in better agreement with the Ar^{q+} - Ne collisions.

Reproduced with permission of the copyright owner. Further reproduction prohibited without permission.

BIBLIOGRAPHY

Afrosimov. V.V., Basalaev, A.A., Panov, M.N., Samoilov, A.V., *Soviet Physics JETP*, **64**, 273 (1986)

Andersson, L. R., *VIth Int. Conf. on the Physics of Highly Charged Ions*, edited by Richard, P., Stockli, M., Cocke, C. L. and Lin, C. D., (American Institute of Physics, New York, 1993), p. 16

Andersson, L.R., Cederquist, H., Barany, L., Liljeby, L., Biedermann, C., Levin, J.C., Keller, N., Elston, S.B., Gibbons, J.P., Kimura, K., and Sellin, I.A., *Phys. Rev. A* **43**, 4075 (1991)

Andersson, L., R., Danared, H., Barany, A., *Nucl. Instrum. and Meth.* B **23**, 54 (1987)

Baskin, S. and Stoner, J.O., *Atomic Energy Levels and Grotrian Diagrams*. North-Holland, Amsterdam, (1978)

Benmeuraiem, L., McCarroll, R. and Opradocle, L. (XV Int. Conf. on Physics of Electronic and Atomic Collisions, Brighton, UK), Abstracts of Contributed Paper, p. 557 (1987)

Cavalcanti, G. H., Gallardo, M., Reyna-Almandos, J. G., Gomide, J. V. B., Trigueiros, A. G., *G. Phys.* B **29**, 6049 (1996)

Cocke, C. L., *J. De. Physique* C1 **50**, 19 (1989)

Cooks, R.G. *Collision Spectroscopy*, Plenum Press, New York, (1978)

Gargaud, M., McCarroll, R., Benmeuraiem, L., *Physica Scr.* **51**, 752 (1995)

Giese, J.P., Cocke, C.L., Waggonover W., Tunnell, L.N., *Physical Review* A **34**, 3770 (1986)

Goldstein, H., *Classical Mechanics* 2nd ed., Addison-Wesley, New York (1980)

Gosselin, A., Ph.D. Dissertation, Universite De Caen (1993), unpublished

Reproduced with permission of the copyright owner. Further reproduction prohibited without permission.

Hansen, G. P., Kocbach, L., Taulbjerg, K., *G. Phys.* B **22**, 885 (1989)

Justiniano, E., Cocke, C.L., Gray, T.J., Dubois, R. Can, C., Waggoner, W., Schuch. R., Schimidt-Boking, H., and Ingwersen, H., *Phys. Rev. A* **29**, 1088 (1984)

Kamber, E.Y., *J. Physics* B **21**, 4185 (1988)

Kamber, E. Y., Cocke, C. L. *Springer Series in Chemical Pysics* **54**, 91 (1991)

Kamber, E.Y., Cocke, C.L., Giese, J.P., Pedersen, J.O.K. and Waggoner, W., *Phys. Rev.* A **36**, 5575 (1987)

Kamber, E.Y., Cocke, C.L., Giese, J.P., Pedersen, J.O.K., Waggoner, W. and Varghese, S.L., *Nuc. Inst. and Methods in Phys. Research* B **24/25**, 288 (1987)

Kimura, M., Iwai, T., Kobayashi, N., Matsumoto, A., Ohtani, S., Okuno, K., Takagi, S., Tawara, H., and Tsurubuchi, S., *J. Phys. Soc. of Japan* 53 **7**, 2224 (1984)

Landau, L.D., *Physics Z. Sovietunion* **2**, 46 (1932)

Lee, A. R., Wilkins, A. C. R., Brenton, A. G., *Rapid Communications in Mass Spectrometry* **9**, 67 (1995)

Mann, R., Folkmann, F., and Beyer H.F., *J. Physics* B **14**, 1161 (1981)

McCullough, R.W., Wilson, S.M., Gilbody, H.B., *J. Physics* B **20**, 2031 (1987)

Meade D. M., *Nucl. Fusion* **14**, 289 (1974)

Moore, C. E., *Atomic Energy Level NBS Circular* No 467, Washington DC. US Goverment Printing Office, (1970)

Muller, A., Salzborn, E., *Phys Lett* A **62**, 391 (1977)

Niehaus, A., *J. Physics* B **19**, 2925 (1986)

Nielsen, E.H., Anderson, L.H., Barany, A., Cederquist, Heinnemeir, J., Hvelplund, P., Knudsen, H., MacAdam, K.B. and Sorensen, J., *J. Physics* B **18**, 1789 (1985)

Nielsen, E. H., Andersen, L. H., Barany, A., Cederquist,H., Hvelplund, P., Knudsen, H., MacAdam, K. B., Sorensen, G., *G. Phys.* B **17**, L139 (1984)

Reproduced with permission of the copyright owner. Further reproduction prohibited without permission.

Okuno, K., Saitoh, H., Soejima, K., Kravis, S., and Kobayashi, N., in Physics of Electronic and Atomic Collisions, edited by Dube, L.J., Mitchell, J.B.A., McConey, J.W., and Brion, C.E. (American Institute of Physics, N.Y., 1995), p. 867

Olson, R.E., *J. Chem. Phys.* **56**, 2979 (1972)

Olson, R.E., Salop, A., *Phys. Rev.* A **14**, 579 (1976)

Opradocle, L., Valiron, P. and McCarroll, R., *J. Phys.* B **16**, 2017 (1983)

Pequignot, D., *Astronomy Astrophysics* **81**, 356 (1980)

Ryufuku, H., Sasaki, K., and Watanabe, T., *Phys. Rev.* A **21**, 745 (1980)

Salop, A., Olson, R. E., *Phys. Rev.* A **13**, 1312 (1976)

Suzuki,K., Okuno, K., Kobayashi, N., *Physica Scripta* T **73**, 172 (1997)

Taulbjerg, K., *J. Physics* B **19**, L367 (1986)

Yaltkaya, S., Kamber, E.Y., and Ferguson, S.M., *Phys. Rev. A* **48**, 382 (1993)

Zener, C., *Prog. R. Soc London* A **137**, 696 (1932)

Reproduced with permission of the copyright owner. Further reproduction prohibited without permission.